ACS OMEGA

http://pubs.acs.org/journal/acsodf

Article

Band Gap Engineering in Two-Dimensional Materials by Functionalization: Methylation of Graphene and Graphene Bilayers

Elham Mazarei, Christopher Penschke, and Peter Saalfrank*

Cite This: *ACS Omega* 2023, 8, 22026−22041

Read Online

ACCESS | Metrics & More | Article Recommendations

ABSTRACT: Graphene is well-known for its unique combination of electrical and mechanical properties. However, its vanishing band gap limits the use of graphene in microelectronics. Covalent functionalization of graphene has been a common approach to address this critical issue and introduce a band gap. In this Article, we systematically analyze the functionalization of single-layer graphene (SLG) and bilayer graphene (BLG) with methyl (CH_3) using periodic density functional theory (DFT) at the PBE+D3 level of theory. We also include a comparison of methylated single-layer and bilayer graphene, as well as a discussion of different methylation options (radicalic, cationic, and anionic). For SLG, methyl coverages ranging from 1/8 to 1/1, (i.e., the fully methylated analogue of graphane) are considered. We find that up to a coverage θ of 1/2, graphene readily accepts CH_3, with neighbor CH_3 groups preferring *trans* positions. Above $\theta = 1/2$, the tendency to accept further CH_3 weakens and the lattice constant increases. The band gap behaves less regularly, but overall it increases with increasing methyl coverage. Thus, methylated graphene shows potential for developing band gap-tuned microelectronics devices and may offer further functionalization options. To guide in the interpretation of methylation experiments, vibrational signatures of various species are characterized by normal-mode analysis (NMA), their vibrational density of states (VDOS), and infrared (IR) spectra, the latter two are obtained from ab initio molecular dynamics (AIMD) in combination with a velocity−velocity autocorrelation function (VVAF) approach.

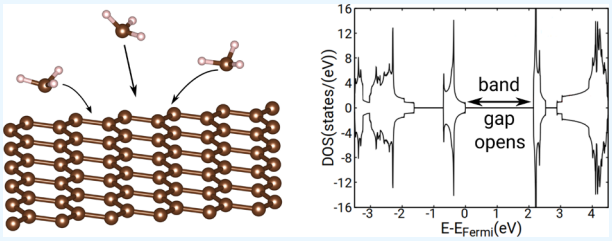

1. INTRODUCTION

Graphene, an extended two-dimensional layer comprising sp^2-hybridized carbon atoms, features remarkable mechanical, electrical, and transport properties.[1−6] It has a high specific surface area[7,8] and large transparency.[9] On top, the material shows special fundamental features, among them the appearance of Dirac cones and pseudorelativistic linear $\underline{k}$-dispersions of bands around them, both associated with the vanishing gap of graphene. Due to the mentioned properties, graphene is known for many (potential) applications in microelectronics, nanotechnology, and analytics.[10] Despite the great potential for applications, it must also be said that pristine graphene, due to its zero band gap and its inertness against chemical reactions, is still limited, e.g., for use as a semiconductor or sensor.

A way to optimize the properties of graphene is by doping, a second one is by substitution of C by other atoms (N, O, etc.), and a third one is by functionalization with atoms or functional groups.[11−16] Functionalization can be covalent, by forming strong bonds with the graphene surface, or noncovalent. Functionalization may also help to avoid agglomeration and restacking to form graphite, for example.[12,17]

Perhaps the simplest form of functionalization is hydrogenation by converting some or all C atoms to C−H groups with sp^3-hybridized carbon, this way possibly transforming graphene from a gapless material to a semiconductor. The fully hydrogenated form, graphane, for example, experimentally first mentioned in ref 18, has a theoretically predicted band gap between 3.5 eV (when computed with PBE[19]) and 4.4 eV (when computed with the hybrid functional HSE06, see below[20]). The band gap can be "tuned" between zero and >4 eV by increasing the level of hydrogenation, according to density functional theory (DFT) calculations and, partially at least, also according to experiments (refs 21 and 22 and references therein). Typically, a certain critical concentration of H is needed to open a band gap.[21] Similar effects were reported after the functionalization of graphene with halogens, OH groups, or oxygen, the latter of which led to graphene oxide or reduced graphene oxide (ref 22 and references therein). The functionalization of bilayer graphene (BLG) is also an active field of research.[23,24] BLG itself is already a material with a nonvanishing band gap, which can further be manipulated by functionalization. The form of BLG with all C atoms rehybridized to sp^3, the two layers connected by C−C bonds, and every second C atom of the layers saturated at the outer

Received: March 28, 2023
Accepted: May 8, 2023
Published: June 5, 2023

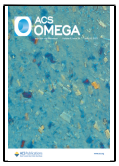

https://doi.org/10.1021/acsomega.3c02068
ACS Omega 2023, 8, 22026−22041

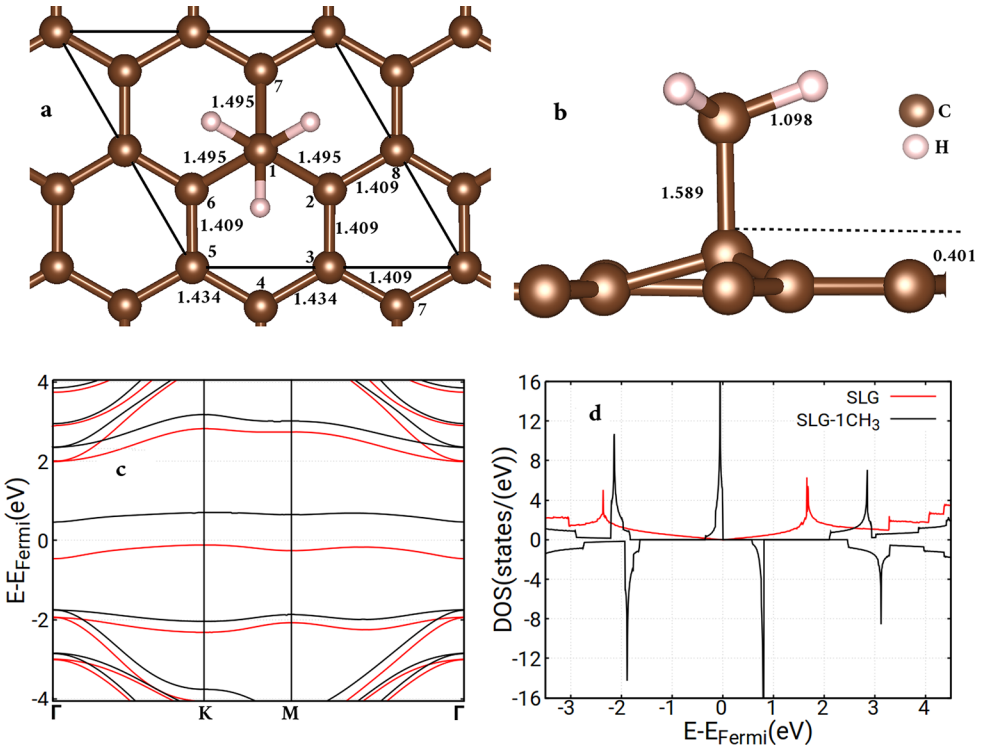

Figure 1. Chemisorption of a single CH_3 radical on SLG. (a) The (2×2) unit cell used for SLG in this work, with atom numbering employed in the text and the CH_3 radical adsorbed on top of C1 (top view, C atoms in dark brown, H in light brown). The PBE+D3 optimized lattice constant of the cell is a = 4.93 Å for "naked" SLG, with a shortest C−C distance of 1.42 Å (Figure 9 in Appendix A). This lattice constant was also used or the calculation of SLG+CH_3, done with PBE+D3/spin-polarized/multiplicity equal to 2 to account for the open-shell character of CH_3. Optimized C−C bond lengths are indicated (all in Å). (b) Side view of (a), with selected bond lengths/distances. (c) Corresponding band structure, with E_{Fermi} indicating the Fermi energy and $\Gamma = (0, 0)$, $K = \frac{2\pi}{3a}(1, 1)$, and $M = \frac{\pi}{a}(1, 0)$. "Spin-up" bands are in red, and "spin-down" bands are in black. (d) Corresponding DOS curves for up-spin (on positive scale) and down-spin (on negative scale) compared to the DOS of pristine SLG (red curve).

sides with H (fully hydrogenated BLG) is called diamane and was, like graphane, first predicted by theory to be a stable large-gap material. It was recently also found in high-pressue experiments, with a reported band gap of 2.8 ± 0.3 eV.[25]

In the present work, we theoretically study the functionalization of single-layer graphene (SLG) and also of BLG with methyl radicals, CH_3. This kind of covalent methylation was achieved by photochemical splitting of precursor molecules containing CH_3 and can be monitored by vibrational spectroscopy, e.g., IR spectroscopy.[26] Nonphotochemical alkylation and arylation of SLG and BLG were also possible, again probed by vibrational spectroscopy.[24] In this latter case, electrophilic species (e.g., methyl cations from methyl halogenides) were involved, and CH_3^+ was added to a (double) layer, which had previously been reduced. Here, in addition to "radicalic' pathways, we also study the "heterolytic" functionalization of SLG by ionic methyl species (CH_3^+ and CH_3^-) with appropriate counterions (Cl^- and Li^+, respectively) included. In general, functionalization of (bilayer) graphene with alkyl and aryl groups not only offers the opportunity to tune the band gap but also opens many possibilities for chemical modification based on C−C bonding.

From the theory side, Li et al.[27] investigated the adsorption of small hydrocarbons like CH_3, CH_4, C_2H_2, C_2H_4, C_2H_6, and C_6H_6 on pristine, doped, and vacancy graphene. For pristine graphene, they state that CH_3 is chemisorbed, while the other species (CH_4, C_2H_2, C_2H_4, C_2H_6, and C_6H_6) are bound by (much weaker) physisorption. Denis et al.[28] theoretically studied the adsorption of different functional groups including CH_3, aryl, C_6H_4, and COOH, on graphene and alkali-doped graphene, where alkali is Li and K. In ref 28, it was concluded that alkali atom doping enhances the chemical reactivity of graphene dramatically.

In the present work, we survey the structures of single-layer graphene (SLG) with different amounts of CH_3 adsorbed at different positions, e.g., on one or at both sides of the 2D material. To this end, density functional theory in the generalized gradient approximation (DFT-GGA) with dispersion corrections is used for periodic models, complemented by hybrid density functional theory. Both physisorption and chemisorption modes of adsorption are considered. For the chemisorbed species, coverages up to one are investigated, where each C atom is saturated with a methyl group positioned on alternating sides of the graphene layer, giving the methyl analogue of graphane, i.e., methyl graphane. Further, chemisorption on bilayer graphene (BLG), and also the adsorption of CH_3^+ and CH_3^- (with counterions included) will be studied. Besides stable structures and adsorption energies, we are interested in optoelectronic properties such as the band gap, band structure, and spin polarization of the materials. In order to guide possible experiments, vibrational spectra are computed by ab initio molecular dynamics (AIMD) combined with the time-dependent correlation function (TCF) approach, giving vibrational density of states (VDOS) curves and IR absorption spectra.

The paper is organized as follows. In section 2, we describe methods and models used for stationary and dynamical (AIMD) calculations. In section 3 we present and discuss results, starting with low-coverage radicalic methylation of SLG (sections 3.1

https://doi.org/10.1021/acsomega.3c02068
ACS Omega 2023, 8, 22026−22041

and 3.2). We then consider high-coverage radicalic methylation of SLG (section 3.3), the methylation of BLG (section 3.4), heterolytic methylations (section 3.5), and finally the impact of methylation on vibrational spectra (section 3.6). A final section 4 concludes and summarizes this work.

2. COMPUTATIONAL DETAILS

2.1. Stationary Calculations. Stationary calculations (geometry optimizations, band structure calculations, and normal-mode analyses) were performed on periodic supercell models using density functional theory (DFT) together with projector augmented wave (PAW) pseudopotentials.[29] The pseudopotential for Li included semicore 1s states. A plane wave basis with a cutoff, V_c, and Monkhorst−Pack $\underline{k}$-point sampling[30] as specified below were adopted. Most calculations were done with the generalized gradient approximation (GGA) functional of the Perdew−Burke−Ernzerhof (PBE) functional,[31] with dispersion corrections included on the D3 level of theory,[32,33] i.e., PBE+D3. For selected cases, the hybrid functional HSE06+D3 was also used.[34,35] All calculations were performed with the Vienna Ab Initio Simulation Package (VASP).[36,37]

We applied (2 × 2 × 1) supercells with eight C atoms for SLG, as shown in Figure 1(a) below. Lateral cell parameters $a = b$ and an angle of $\gamma = 120°$ between them were adopted. For SLG, a lattice constant $a = 4.93$ Å is found on the PBE+D3 level, corresponding to a shortest C−C distance of 1.42 Å. These lattice constants were kept for low coverages with methyl, but reoptimized with PBE+D3 when many methyl groups were adsorbed (coverage $\theta > 1/2$), leading to elongated lattice constants (see below), always with the restriction $a = b$ and $\gamma = 120°$. In every case, all atom positions were optimized. A fixed vacuum gap, $c = 20.76$ Å, was used for SLG. For BLG, the (2 × 2) cell consists of two layers (16 C atoms, see below) and $c = 20.00$ Å was chosen. A Γ-centered grid 11 × 11 × 1 was used for geometry optimization, while for the calculation of electronic densities of states (DOS) denser meshes (44 × 44 × 1 for SLG and 33 × 33 × 1 for BLG) were employed. A plane-wave cutoff $V_c = 700$ eV was chosen throughout.

To SLG (or BLG) were added methyl groups, and the geometries were optimized. Both spin-unpolarized and spin-polarized calculations were performed, with various spin multiplicities. Different initial geometries (e.g., "from below" or "from above") were chosen, and different adsorption situations were considered (physisorption or chemisorption). Depending on the initial geometry and the mode of computation (spin-polarized or not, different spin multiplicities), one obtains different minima and energies. As an example, in Figure 1(a and b) below, the chemisorption of a single CH_3 radical above one of the graphene C atoms is illustrated, with the geometry optimized on the spin-polarized PBE+D3 (multiplicity of 2) level (see section 3.1).

Besides geometries and adsorption energies, band structures and DOS curves were also determined, and from the latter band gaps were also determined, separately for electrons with α ("up") or β ("down") spin in case of spin-polarized calculations. Additionally, normal mode analyses (NMA) were performed to obtain vibrational frequencies in the harmonic approximation.

2.2. AIMD and Vibrational Spectra Calculation. For vibrational spectra beyond the uncoupled harmonic approximation and also to include finite temperature effects, we performed ab initio molecular dynamics (AIMD) simulations using VASP. Trajectories were run for canonical ensembles (NVT) using PBE+D3 and a Nosé−Hoover thermostat held at $T = 298.15$ K (room temperature).[38] We propagated the equations of motion for (all) nuclear degrees of freedom using the velocity-Verlet algorithm with a time step of 0.5 fs. For each studied system, we first ran a 5 ps trajectory for equilibration, starting from the optimized structure. From these equilibrated structures, four trajectories were run, each 5 ps long. In every trajectory, the last 3 ps were used for sampling, i.e., 12 ps in total.

Vibrational density of states (VDOS) curves were obtained from Fourier transformed velocity−velocity autocorrelation functions (VVAFs) as[39]

$$\mathrm{VDOS}(\omega) \propto \sum_{i=1}^{N} \int_0^\infty \langle \underline{v}_i(0) \cdot \underline{v}_i(t) \rangle \mathrm{e}^{-i\omega t}\, \mathrm{d}t \tag{1}$$

Here, $\underline{v}_i(t)$ is the velocity of atom i at time t, N is the total number of moving atoms, and $\langle \underline{v}_i(0)\, \underline{v}_i(t) \rangle$ is a VVAF averaged over different trajectories. The latter was computed as described in greater detail in ref 40.

Further, we calculated infrared (IR) spectra from the first-order optical susceptibility, χ^1, the latter obtained from the Fourier transform of the dipole−dipole autocorrelation function. In order to compute the dipole−dipole correlation function, we use an efficient, VVAF-only method suggested by Ohto et al.,[41] applying it to the C−C vibrations (within the graphene layer(s) or between accepting graphene C and adsorbed methyl) of the systems under study. Using this method, the first-order susceptibility needed for IR spectra can be written as[40,41]

$$\chi^{(1)}_{\mathrm{ab}}(\omega) = \frac{Q(\omega)\mu'^{\,2}_{\mathrm{CC}}}{i\omega^2} \int_0^\infty \sum_i^M \sum_j^M \langle v^{\mathrm{CC}}_{b,j}(0) v^{\mathrm{CC}}_{a,i}(t) \rangle \mathrm{e}^{-i\omega t}\, \mathrm{d}t \tag{2}$$

Here, $v_{a,i} = \dot{r}_{a,i}$ is the a-th component (= x, y, z; z perpendicular to the surface and x and y being in the surface plane) of the velocity vector of CC bond i, the time-derivative of the coordinate vector $\underline{r}_i(t) = (x_i(t), y_i(t), z_i(t))$ of that bond. Altogether, M oscillators are considered. In the latter equation, we have also introduced a quantum correction factor[41] $Q(\omega) = \frac{\hbar\omega}{k_B T} / (1 - e^{-\hbar\omega/k_B T})$. Derivatives of (dynamical, i.e., ω-dependent) dipole moments, $\mu'_{\mathrm{CC}}(\omega)$ with respect to the vibrational coordinate are treated here as constant (their ω-dependence is neglected). IR intensities will be given in arbitrary units and normalized as described below.

In particular, IR spectra with light polarized along the z-direction will be computed from the real part of the first-order susceptibility as $I^{\mathrm{IR}}_z(\omega) \propto \mathrm{Re}\{\chi^{(1)}_{zz}(\omega)\}$. We work in full analogy to the methodology (and with codes) described in ref 40, where further details can be found.

3. RESULTS AND DISCUSSION

3.1. Functionalization of a Single Graphene Layer with One Methyl Group: Coverage 1/8. We start with the adsorption of a single methyl radical per (2 × 2) unit cell, corresponding to coverage 1/8. Using the same fixed lattice parameters as for SLG ($a = b = 4.93$ Å, $\gamma = 120°$), attaching a single CH_3 radical to one of the SLG C atoms, and optimizing all atom positions gives the structure shown in Figure 1(a and b), at the PBE+D3 spin-polarized (spin multiplicity of 2; in this case, the magnetic moment of the unit cell is 1 μ_B).

Accordingly, the methyl group attaches in "staggered" fashion, perpendicular on top of the accepting C atom (C1), with a C−C

https://doi.org/10.1021/acsomega.3c02068
ACS Omega 2023, 8, 22026−22041

Table 1. Single CH_3 Radical Chemisorbed on (2 × 2)-SLG (Coverage 1/8): Comparison of Two Different Functionals Used Respectively for the Energetics and the Band Structure[a]

	energetics			band structure			
method	ΔE_1^c	ΔE_1^p	ΔE_{TS}	$\Delta_\uparrow$	$\Delta_\downarrow$	Δ_{tot}	gap type
PBE+D3	−0.35	−0.02	+0.20	2.10	2.21	0.57	indirect (K, Γ)
HSE06+D3	−0.44	−0.13	+0.25	3.25	3.38	1.85	indirect (Γ, K)

[a] $\Delta E_1^{c,p}$ denotes chemisorptive and physisorptive adsorption energies, ΔE_{TS} is the transition state energy relative to the SLG + CH_3 asymptote, $\Delta_\uparrow$ is the spin-up gap, $\Delta_\downarrow$ the spin-down gap, and Δ_{tot} is the total gap. All energies are in eV. .

distance of 1.59 Å, slightly longer than a typical C−C single bond (1.54 Å). The C−C bond lengths within the SLG layer are elongated around the accepting C1 (with bond lengths C1−C2 of 1.50 Å compared to the 1.42 Å for SLG without adsorbate), slightly shortened for the more distant C2−C3 bonds (1.41 Å), and slightly elongated for most distant C3−C4 bonds (1.43 Å), cf. Figure 1(a). Additionally, the accepting C atom is lifted out of the plane (Figure 1(b)) by 0.40 Å, all indicating the $sp^2 \rightarrow sp^3$ rehybridization of C1 and all in good agreement with previous theoretical work.[27]

The adsorption energy for accepting a single CH_3 was calculated as

$$\Delta E_1 = E_{SLG-CH_3} - (E_{SLG} + E_{CH_3}) \quad (3)$$

Here, E_{SLG-CH_3} is the energy of the adsorbed system, E_{SLG} is the energy of the SLG layer, and E_{CH_3} is the energy of the free CH_3 radical, the latter of which was calculated by placing the radical in a cell of the same size as for the adsorbed species. On the (spin-polarized) periodic PBE+D3 level of theory, $\Delta E_1 = -0.35$ eV, cf. Table 1. This indicates, together with the elongated C1−C(CH_3) bond (1.59 Å), a rather weak covalent bond due to chemisorption. On the same level of theory, we also find a physisorbed state, where CH_3 adsorbs as a flat molecule also on top of C1 farther away from the surface with a C1−C(CH_3) "bond" length of 3.22 Å and an adsorption energy of −0.02 eV, see Table 1. The physisorbed state is reached from the gas phase without a barrier, but a barrier exists between the physisorption and the chemisorption well; using the DIMER method, implemented in VTSTTools,[42] a transition state was found with a barrier of 0.22 eV from the physisorbed side or 0.20 eV above the SLG+CH_3 asymptote. In the literature, theoretical work was reported with a qualitatively similar outcome, i.e., physisorption and chemisorption states and barriers between them.[27,43−45] Quantitatively, adsorption energies and barriers were slightly different, mostly due to other coverages or other electronic structure methods and models in the literature.

While free-standing SLG is a semimetal with zero band gap, for the free-standing SLG with one methyl radical chemisorbed a band gap opens. This can be seen from the spin-polarized (multiplicity of 2) bandstructure in Figure 1(c). The band structure consists of pairs, with band pairs in Figure 1(c) reflecting bands for up- (in red) and down-spin electrons (black), respectively. The two flat bands close to the Fermi level give rise to the density of states (DOS) curves shown in Figure 1(d) (with a positive scale for spin-up and a negative scale for spin-down). A "total band gap" (the energy difference of the down-spin conduction band minimum (CBM) at the Γ-point, and the up-spin valence band maximum (VBM) at the K-point) of 0.57 eV is found on the PBE level of theory. One also finds spin-resolved bands gap of 2.10 and 2.21 eV for spin-up and spin-down, cf. Table 1. Closer inspection of the (atom-) projected density of states (PDOS) shows that both the occupied spin-up band right below the Fermi level and the first unoccupied spin-down above the Fermi level are dominated by (the p_z-orbitals) of C atoms in the *ortho* position (and to a lesser extend in *para* position) relative to the accepting C atom, C1. These atoms are therefore centers with the highest spin density, corresponding to unpaired electrons, as expected from simple chemical resonance structures. In addition, the C atom of the CH_3 contributes to the DOS close to E_{Fermi} (but not the accepting C atom).

It is known that GGA functionals underestimate band gaps. To check this for methylated SLG, we also applied the HSE06 hybrid functional[34,35] with the D3 correction to recalculate the band structure, adsorption energies, and adsorption geometries. It is found that indeed the total gap becomes considerably larger with HSE06 and the band structure shows also some qualitative difference, namely, the VBM of spin-up is now at Γ and the CBM for spin-down is now at K (not shown), opposite to what was found for PBE+D3. On the HSE06+D3 level, the total band gap is 1.85 eV. Additionally, the chemisorption (−0.44 eV) and physisorption energies (−0.13 eV) are somewhat larger for HSE06+D3, and so is the transition state energy (+0.25 eV), which makes barriers for transitions between the two states larger for HSE06+D3 (geometries are similar for both functionals.) While HSE06+D3 is expected to be more accurate, we will use PBE+D3 for the more systematic studies below, simply because the former is computationally very costly and because trends should still be reliable already on the PBE+D3 level. It should be kept in mind, however, that computed absolute band gaps are probably systematically underestimated in what follows.

3.2. Functionalization of a Single Layer of Graphene with Two Methyl Groups: Coverage 1/4. We also studied the chemisorption of from two to eight methyl radicals on a free-standing SLG, (2 × 2) unit cell, corresponding to coverages from 1/4 to 1, respectively, and giving rise to what we call SLG-*n*CH_3 in what follows (with $n = 2-8$, and also including $n = 0$ and 1 for completeness). Considering two CH_3 groups first, and starting from the SLG-1CH_3 structure in Figure 1, we have the choice to add the second methyl on top of C atoms in positions 2 (nearest neighbor, "*ortho*" position), 3 (second-nearest neighbor, "*meta*" position), and 4 (third-nearest neighbor, "*para*" position). Other positions, namely, 5, 6, 7, and 8, give no other structures by symmetry. Further, we have the possibility to add the second CH_3 on the same side as the first one, "up" or on the opposite side of SLG, "down" in what follows, giving combinations "up−up" or "up−down" for SLG-2CH_3. Finally, we can perform spin-unpolarized or spin-polarized calculations, in the latter case with multiplicity, $M = 1$ or 3.

We first of all find that, not surprisingly, spin-polarized $M = 1$ and spin-unpolarized calculations give the same structures and energies (up to very small deviations), the latter measured in analogy to eq 3 by an adsorption energy for the second methyl as ($n = 2$)

https://doi.org/10.1021/acsomega.3c02068
ACS Omega 2023, 8, 22026−22041

$$\Delta E_n = E_{\mathrm{SLG}-n\mathrm{CH_3}} - (E_{\mathrm{SLG}-(n-1)\mathrm{CH_3}} + E_{\mathrm{CH_3}}) \quad (4)$$

Equation 4 will later be used to also compute the nth adsorption energy for $n > 2$, i.e., the energy change when adding one more CH_3 to SLG-$(n-1)CH_3$. In Table 2, we show ΔE_2 for different

Table 2. Chemisorption of a Second CH_3 Radical on (2×2)-SLG (Coverage 1/4): Comparison of Different Structures (1-2, 1-3, and 1-4; "Up" (u) and "Down" (d)) and Spin Multiplicities ($M = 1$ or $M = 3$)[a]

structure/ multiplicity	uu-12, $M = 1$	uu-12, $M = 3$	ud-12, $M = 1$	ud-12, $M = 3$
ΔE_2	−0.07	+1.45	−2.31	−0.25
Δ_{tot}			0.09	
structure/ multiplicity	uu-13, $M = 1$	uu-13, $M = 3$	ud-13, $M = 1$	ud-13, $M = 3$
ΔE_2	+0.52	−0.11	+0.17	−0.23
Δ_{tot}				0.68
structure/ multiplicity	uu-14, $M = 1$	uu-14, $M = 3$	ud-14, $M = 1$	ud-14, $M = 3$
ΔE_2	+0.48	−0.11	−1.70	+1.14
Δ_{tot}			3.50	

[a]See text for the nomenclature. Shown are ΔE_2 and selected total band gaps Δ_{tot} (both in eV) obtained from spin-polarized PBE+D3 calculations after geometry optimization; however, at fixed lattice parameters $a = b = 4.93$ Å and $\gamma = 120°$.

optimized structures (on the PBE+D3 level). These structures are labeled as "ud-13 ($M = 3$)" for example, to characterize an "up−down" structure with two methyls, one above C1 and one below C3 ("*meta*"), with multiplicity $M = 3$.

From the table, we note that (i), as expected, "up−down" geometries are usually favored over "up−up" geometries (except for 1−3, $M = 3$ species). (ii) For "up−down", $M = 1$ multiplicities are always more stable than higher multiplicities (except for 1−3), giving rise to nonmagnetic states, since the DOS curves for spin-up and spin-down are also the same (see below). (iii) The most stable system for "up−down" $M = 1$ is "ud-12", followed by "ud-14" and "ud-13". In line with our findings, Denis et al.[46] reported that functional groups have a strong tendency to adopt the ortho-up−down functionalization pattern because it reduces the deformation energy.

Note that the most stable "ud-12, $M = 1$", exhibits a much larger second adsorption energy, $\Delta E_2 = -2.30$ eV, than the first one, $\Delta E_1 = -0.35$ eV. In fact, a stable C−C single bond is formed for SLG-$2CH_3$ (ud-12) between C1 and C2, embedded in a "sea" of delocalized π-electrons, as visualized in Figure 9(b) in Appendix A, where $r_{C1-C2} = 1.56$ Å is found. In contrast, for SLG-CH_3 an energetically unfavorable "dangling electron" remains. In Figure 2 we show sideviews of structures of SLG-nCH$_3$ for $n = 1$ and 2 (and also for $n = 3-8$). From panel (b) there, corresponding to "ud-12", we note that the two accepting C atoms C1 and C2 have a quasi-tetrahedral coordination shell, indicating their sp^3-rehybridization, while nonaccepting C atoms are still in the plane originally spanned by SLG.

Turning to the electronic structure of SLG-$2CH_3$, from Table 2 we also note that the most stable three "up−down, $M = 1$" structures show different band gaps. The most stable "ud-12, $M = 1''$, has a very small gap with <0.1 eV, if one at all. In fact, the small finite band gap is numerical in nature: increasing the number of $\underline{k}$-points from $33 \times 33 \times 1$ to $44 \times 44 \times 1$ decreases the band gap (not shown), and also the band structure, given in Appendix A in Figure 10(b) for ud-12, is gapless. The bands shown in bandstructure figures are from energies interpolated between different $\underline{k}$-points, while computed (and tabulated) band gaps are taken from DOS curves. Among higher-energy forms, "ud-13, $M = 1$" has a similar, finite band gap as SLG-$1CH_3$ (0.57 eV, see Table 1), and "ud-14, $M = 1$" has an even much larger gap (3.50 eV). From Figure 3(b), where we show electronic density of states curves for the most stable forms of SLG-nCH$_3$ ($n = 1-8$) that we found, in comparison to the DOS of SLG we see the (numerically) very small gap for the most stable SLG-$2CH_3$ (ud-12, $M = 1$). Note also from there that indeed no spin-polarization occurs in this case, i.e., DOS(spin-up) = DOS(spin-down). In contrast, for SLG-$1CH_3$ in Figure 3(a) (or Figure 1(d), where it was also shown), the two already rather localized "midgap" states are visible, one occupied (for spin-up) and one empty (for spin-down) and shifted, causing a distinct band gap. The corresponding band structure for SLG-$1CH_3$ is shown in Figure 1(c) and also in Appendix A, Figure 10(a), while Figure 10(b−h) gives the band structures for SLG-nCH$_3$ ($n = 2-8$, respectively).

3.3. Functionalization of Single Layer of Graphene with More than Two Methyl Groups: Higher Coverages.

We now consider the cases of SLG-nCH$_3$ with $n = 3-8$ per (2×2) cell, corresponding to coverages from 3/8 (for $n = 3$) to 1 (for $n = 8$), the latter being the methylated analogue to graphane. For $n = 3$ and 4, during geometry optimization lattice parameters were still fixed at $a = b = 4.93$ Å and $\gamma = 120°$, but all atom positions were optimized. For both, minima are found for different positions of the methyl groups and different spin multiplicities. For $n = 5-8$, on the other hand, the systems become gradually "overcrowded" and finding stable minima becomes cumbersome or impossible unless also the lattice parameters are adjusted. Thus, in these cases we also optimized lattice parameters, however, under the constraints $a = b$ and $\gamma = 120°$.

In Figures 2(c−h) (and 9(c−h) in Appendix A), the found most-stable structures are shown also for $n = 3-8$, respectively, as side (and top) views. We note that for odd n ($n = 1$, 3, 5 and 7) the most stable spin multiplicity is $M = 2$ on the PBE+D3 level of theory, while the most stable spin multiplicity is $M = 1$ for the even n ($n = 0$, 2, 4 and 8). For the latter, also no differences between spin-polarized and spin-unpolarized calculations are found, and DOS(up-spin) = DOS(down-spin) according to Figure 3. The structures shown in Figures 2 and 9 are, using an obvious notation, of the type udu-123 for $n = 3$, udud-1234 for $n = 4$, ududu-12345 for $n = 5$, udududu-123456 for $n = 6$, udududu-123457 for $n = 7$, and udududud-12345678 for $n = 8$ (the graphane analogue). These structures were found to be the most stable ones among three structures studied for $n = 3$ (namely, udu-123, udu-128, and udd-126), five structures for $n = 4$, two structures for $n = 5$, and two structures for $n = 6$. For $n = 7$ and 8, only one structure has been optimized.

From the figures, the following is found: (i) Up to $n = 4$ (with "normal" unit cell sizes), the methyl groups can largely avoid each other and bond lengths, as well as buckling behavior, indicate that the accepting C atoms rehybridize to sp^3 and form single C−C bonds between them. (ii) For $n > 4$, the situation is more complicated. The lattice parameters widen considerably and C−C single-bond lengths (in the SLG) layer also become larger, with very large values of r_{C-C} between 1.62 and 1.83 Å (for one C−C bond in case of SLG-$7CH_3$). (iii) The average buckling of the systems increases with increasing n. (iv) CH_3 groups are slightly tilted (not perpendicular to the SLG plane) for $n > 1$.

https://doi.org/10.1021/acsomega.3c02068
ACS Omega 2023, 8, 22026−22041

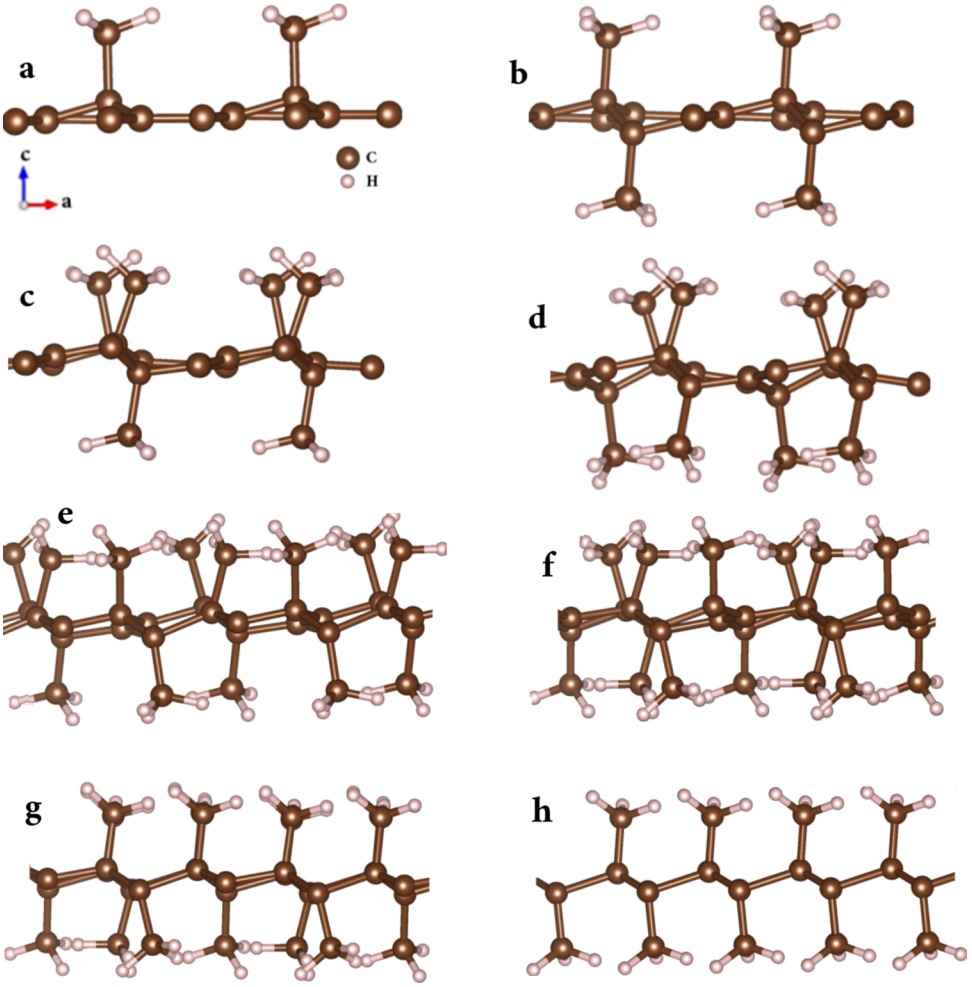

Figure 2. Side view of optimized most-stable found structures of SLG-nCH$_3$ (from n = 1 to n = 8) for (2 × 2) unit cells used in this work. For n = 1−4, the lattice parameters were fixed at $a = b = 4.93$ Å and $\gamma = 120°$ (the optimized values of free-standing SLG), while for the n = 5−8 lattice parameters were reoptimized (see text). All calculations are done using spin-polarized PBE+D3, for multiplicities M = 2 (for n = 1 (a), 3 (c), 5 (e), and 7 (g); in these cases, the magnetic moment of the unit cell is 1 μ_B) or M = 1 (for n = 2 (b), 4 (d), 6 (f), and 8 (h); in these cases, the magnetic moment of the unit cell is 0 μ_B).

While large C−C bond lengths (up to ∼1.8 Å) are known for certain very crowded but still stable organic molecules,[47] we find that for methylated SLG, beyond a coverage of 1/2 (or n = 4 in our case), it becomes energetically quite challenging to add further methyl groups. This is demonstrated in Figure 4(a) where, for the structures shown in Figures 2 and 9, the energy changes ΔE_n to add one more methyl group to SLG-(n − 1)CH$_3$, defined in eq 4, are plotted as a function of n and listed in Table 3. It is seen that, for odd n (>2), adding one more methyl is energetically unfavorable, and in particular for n = 5 and 7 the energy cost is more than 2 eV, not even counting possible additional barriers. As for n = 1 and n = 2, one further notes that creating even-n species is energetically favored. One may also define an average adsorption energy per methyl group, i.e.,

$$E_{ads} = \frac{1}{n}[E_{SLG-nCH_3} - (E_{SLG} + nE_{CH_3})] \quad (5)$$

with values given in Table 3. This latter measure supports the statements just made, with even-n species being relatively more stable, a general destabilization for large n (in particular for n > 4), and an exceptional instability for n = 7, due to extraordinary C−C bond lengthening in combination with an unpaired electron (cf. Figure 9 in Appendix A).

When considering the band structure of the species with n = 1−8, we see from Figure 4(b), where the total band gaps are shown, and also from Table 3, where they are listed, the overall trend of increasing band gap with increasing n, in line with the gradual destruction of the conjugated π-electron system when more and more C atoms rehybridize to sp^3. One also notes an oscillatory behavior of the gap, with particularly small gaps for n = 2, 3, 5, and 7, and very large gaps for n = 4, 6, and 8. From the DOS curves in Figure 3, we see that all even-n species are spin-unpolarized, forming "singlets", while all odd-n species show spin-polarization in their M = 2 ground state.

Table 3 also lists other properties of SLG-nCH$_3$, like spin-resolved band gaps and utilized lattice constants. While SLG-7CH$_3$ is particularly unstable, the methylated form of graphane, SLG-8CH$_3$, has a thermodynamic tendency to form, as indicated by the negative (albeit small) adsorption energy per CH$_3$, E_{ads}. The methylated graphane structure shown in Figures 2 and 9 is a "chair" conformer, whose hydrogenated (graphane) analogue was predicted to also be the most stable form of graphane.[19] For methyl graphane, however, the ligands (CH$_3$) are slightly tilted. The PBE+D3 band gap for this species is 3.14 eV, and it is direct, as also predicted for graphane.[19,20] For comparison, as mentioned earlier the computed band gap of graphane is

https://doi.org/10.1021/acsomega.3c02068
ACS Omega 2023, 8, 22026−22041

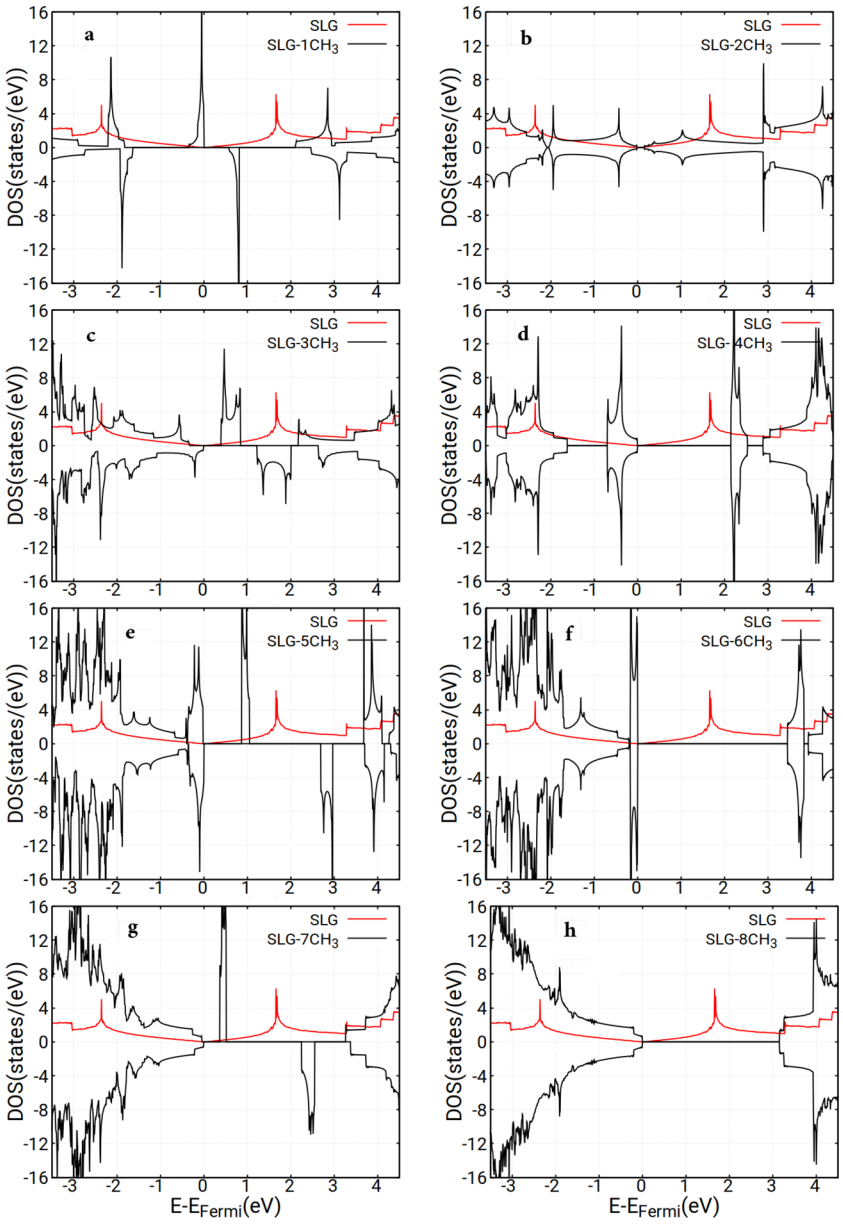

Figure 3. Electronic density of states (DOS) curves of optimized most-stable found structures of SLG-nCH$_3$ (from n = 1 to n = 8) for (2 × 2) unit cells used in this work. All calculations are done with PBE+D3 and M = 2 (in the case of n = 1 (a), 3 (c), 5 (e), and 7 (g)), and M = 1 (in the case of n = 2 (b), 4 (d), 6 (f), and 8 (h)). For the latter, no spin-polarization can be seen, i.e., DOS(spin-up) = DOS(spin-down). In all panels, the DOS of SLG from a spin-unpolarized PBE+D3 is shown in red for comparison.

between 3.5 (on the PBE level[19]) and 4.4 eV (with HSE06[20]). Further, the band gap of diamond is around 4.3 eV when computed with PBE, 5.3 eV on the HSE06 level, and around 5.5 eV experimentally.[48] We therefore anticipate a band gap ordering of Δ_{tot}(methyl graphane) < Δ_{tot}(graphane) < Δ_{tot}(diamond).

3.4. Adsorption of One or Two Methyl Groups to Bilayer Graphene. We also studied adsorption of methyl groups on bilayer graphene, an experimentally well-known 2D material. BLG is modeled as a free-standing bilayer, in the particular stable AB (Bernal) stacking. The interlayer distance was optimized on the PBE+D3 level using (2 × 2) unit cells, now with 16 C atoms, assuming lattice parameters $a = b$ = 4.93 Å and γ = 120° as earlier (c = 20 Å). For other computational parameters, see section 2.1.

BLG can be functionalized at the outside(s) of or inside the bilayer. We have studied low-coverage situations only, with one CH_3 per (2 × 2) cell adsorbed either "outside" or "inside" or with two methyl groups adsorbed, one "outside" and the other one "inside", both attached to the same layer. Again, spin-unpolarized and spin-polarized calculations with different multiplicities were tested, as well as different adsorption sites for BLG-2CH$_3$.

Starting with BLG-1CH$_3$ "outside", we find physisorption and chemisorption wells when approaching one C atom of one of the layers. The resulting geometries are similar to those found for SLG-1CH$_3$, as shown for the chemisorbed species in Figure 5(a). For this arrangement the interlayer distance D is 3.32 Å according to the figure, which is close to the value for pristine BLG. Note that the interlayer distance, indicated by dashed lines in Figure 5 (also for other methylated BLG species), varies

https://doi.org/10.1021/acsomega.3c02068
ACS Omega 2023, 8, 22026−22041

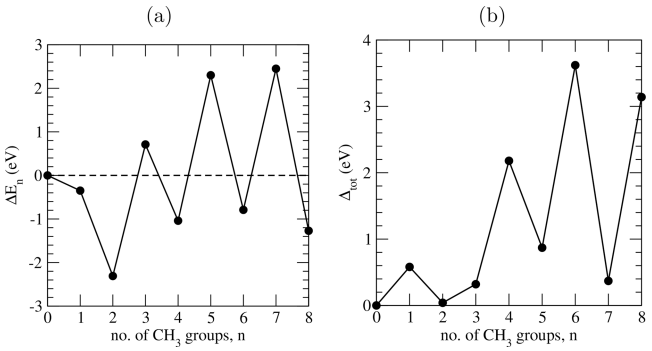

Figure 4. (a) Energy change ΔE_n as a function of n to add one more methyl group to SLG-$(n-1)$CH$_3$, as defined in eq 4, for all structures shown in Figure 2 (and Figure 9). (b) Total gap Δ_{tot} for the same structures. All values calculated at the PBE+D3 level of theory.

Table 3. Properties of SLG-nCH$_3$[a]

n	a	ΔE_n	E_{ads}	$\Delta_\uparrow$	$\Delta_\downarrow$	Δ_{tot}	gap type
1	4.93	−0.35	−0.35	2.10	2.21	0.57	indirect (K, Γ)
2	4.93	−2.31	−1.33	0.09	0.09	0.09	indirect (K, Γ)
3	4.93	+0.71	−0.65	0.70	1.22	0.40	direct (Γ)
4	4.93	−1.04	−0.75	2.15	2.15	2.15	indirect (K, Γ)
5	5.36	+2.30	−0.14	0.89	2.68	0.87	indirect (K, Γ)
6	5.47	−0.79	−0.25	3.62	3.62	3.62	direct (Γ)
7	5.63	+2.45	+0.14	0.41	2.24	0.37	direct (Γ)
8	5.81	−1.27	−0.04	3.14	3.14	3.14	direct (Γ)

[a] $a(=b)$ is the lattice constant adopted or optimized, ΔE_n is the adsorption energy when adding one extra CH$_3$ to SLG-$(n-1)$CH$_3$, E_{ads} is the adsorption energy per methyl group relative to the SLG +CH$_3$ asymptote, $\Delta_\uparrow$ is the spin-up gap, $\Delta_\downarrow$ is the spin-down gap, and Δ_{tot} is the total gap. All energies are in eV, the lattice constant are in Å.

slightly depending on which C atoms are chosen for distance measurements because the methylated layer is not ideal flat. Additionally, the physisorption, chemisorption and transition state energies are very similar to SLG-1CH$_3$, as can be seen from comparing the $\Delta E_1^{p,c}$ and ΔE_{TS} values of Table 4 (entry "BLG-1CH$_3$, outside") with the corresponding PBE+D3 values of Table 1 for SLG-1CH$_3$. Like for SLG-1CH$_3$, for BLG-1CH$_3$ (outside) the most stable spin state also has multiplicity $M = 2$. Note that in contrast to SLG-1CH$_3$, only a small gap of ∼0.07 eV is found for BLG-1CH$_3$. This is consistent with a symmetry breaking in BLG by functionalization, similar to small-gap openings in BLG by symmetry breaking caused by a gate voltage, a surface on which BLG is adsorbed, or doping.[49] The gap is small due to the second graphene layer remaining almost intact, only weakly interacting with the first layer. As a consequence, also the electronic density of states curve of BLG-1CH$_3$ is essentially the sum of the DOS of graphene and SLG-1CH$_3$, as can be seen from Figure 6(a). This is further reflected by the band structure itself, shown in Figure 11(a) in Appendix B.

The situation is different for BLG-1CH$_3$ "inside". To accommodate CH$_3$ between the layers, by chemical bonding, the bilayer has to widen, and the interlayer distance increases from 3.32 to 5.20 Å (between two C atoms, as shown in Figure 12(a) in Appendix B). As can be seen from Table 4, the adsorption energy is much smaller than that for BLG-1CH$_3$ "outside", as one might expect, due to the loss of van der Waals attraction between the more distant graphene layers. The computed band gap is vanishingly small (or zero), again since the second, nonfunctionalized layer is still intact. The corresponding DOS curves and band structure are shown in Figure 12(b and c) in Appendix B.

When adsorbing a second methyl group, we consider only the case of adsorption on one of the two layers. This could be the "upper layer" in case BLG is mounted on a surface. Among several possibilities studied, the most stable configurations are ud-12, ud-13, and ud-14 with multiplicity, $M = 1$, giving spin-unpolarized situations. The geometries of ud-12, ud-13, and ud-14 are shown in Figure 5 as side views. The corresponding second adsorption energies, ΔE_2 in Table 4, indicate similar values as those of the most stable SLG-2CH$_3$ species in Table 2. The most stable form is ud-12, followed by ud-14 and ud-13 as before. From the table, we also note that the total gaps are very small (of the order of those found here numerically for free-standing BLG, which is 0.004 eV), simply because the second graphene layer still remains almost intact. Here also the resulting DOS curves in Figure 6 can be interpreted as arising from the sum of the DOS curves of SLG-2CH$_3$ and the one of graphene (see, for example, Figure 3(b)).

3.5. Methylation of Graphene by Heterolytic Reactions: Methyl Anion and Methyl Cation. So far, we considered methylation only via a homolytic route, i.e., reaction with methyl radicals. An alternative route would be heterolytic in nature by splitting CH$_3$X (with X = halogen, for example) into CH$_3^+$ and X$^-$ and attaching the methyl cation to SLG or BLG. Similarly, one could split CH$_3$M (with M = alkali, for example) heterolytically into CH$_3^-$ and M$^+$ and attaching the methyl anion. Here we study both routes by adding one or two methyl cations or anions to a SLG graphene layer, using (2×2) unit cells as before. As counterions we use Cl$^-$ (corresponding to the splitting of CH$_3$Cl) or Li$^+$ (corresponding to the splitting of CH$_3$Li), respectively.

The reaction energy for first heterolytic methylation is calculated as

$$\Delta E_1 = E_{\mathrm{SLG-CH_3^{+/-}+Cl^-/Li^+}} - (E_{\mathrm{SLG}} + E_{\mathrm{CH_3+Cl/Li}}) \quad (6)$$

Here, $E_{\mathrm{SLG-CH_3^+ + Cl^-}}$ is the energy of SLG-CH$_3^+$ with a Cl$^-$ counterion nearby, and $E_{\mathrm{SLG-CH_3^- + Li^+}}$ is that of SLG-CH$_3^-$ with a Li$^+$ counterion. Further, E_{SLG} and $E_{\mathrm{CH_3+Cl/Li}}$ are energies of the starting materials, SLG and *homolytically dissociated* CH$_3$Cl or CH$_3$Li, respectively, used as reference species here (i.e., as reactants after photolytic splitting of CH$_3$Cl or CH$_3$Li). The latter was calculated from optimizing CH$_3$ with Cl and Li at a large distance from CH$_3$ using the same unit cell parameters as those for SLG-CH$_3^{\pm}$+Cl$^-$/Li$^+$. Note that also for radicalic methlyation in previous chapters we did not include the energy costs to create methyl radicals prior to attachment to SLG and BLG, so the comparison based on eq 6 is fair. We remark that the homolytic dissociation energies of CH$_3$Cl and CH$_3$Li are around 3.7[50] and 2.0 eV,[51] respectively, according to high-level ab initio calculations. Note finally that the anticipated assignment of charges for the product is somewhat formal so far, see below for this issue. Expressions similar to eq 6 hold for adding a second CH$_3$ anion or cation, with a reaction energy ΔE_2, in which case two counterions are needed per unit cell. Again, different adsorption sites or combinations of adsorption sites were considered. Although the number of electrons is even in all cases, both spin-unpolarized and spin-polarized calculations were performed, the latter with different spin multiplicities.

In Figure 7 we show stable structures found on the PBE+D3 level for SLG-CH$_3^+$+Cl$^-$ (a), SLG-2CH$_3^{2+}$+2Cl$^-$ (b), SLG-

https://doi.org/10.1021/acsomega.3c02068
ACS Omega 2023, 8, 22026−22041

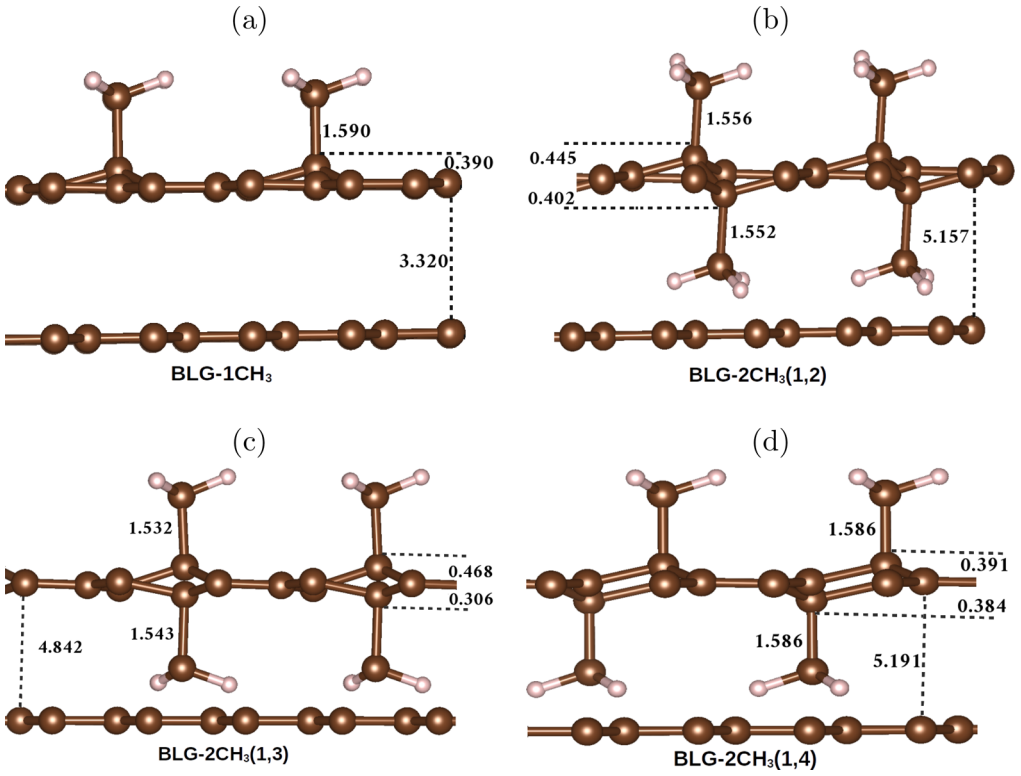

Figure 5. Side views of (a) BLG-1CH_3 (outside), (b) ud-12 BLG-2CH_3 (named here BLG-2CH_3(1,2)), (c) ud-13 BLG-2CH_3, and (d) ud-14 BLG-2CH_3 optimized at the PBE+D3 level of theory. Some bond lengths, out-of-plane displacements, and interlayer distances (in Å) are indicated.

Table 4. Single CH_3 Radical Chemisorbed on (2 × 2)-BLG (BLG-1CH_3) Either "Outside" of One Layer or "Inside" Between the Layers[a] and Similar (Selected) Information for the Three Forms of BLG-2CH_3 Shown in Figure 5 ud-12, ud-13, and ud-14[b]

	energetics			band structure				
BLG-1CH_3	ΔE_1^c	ΔE_1^p	ΔE_{TS}	$\Delta_\uparrow$	$\Delta_\downarrow$	Δ_{tot}	gap type	D
outside	−0.34	−0.03	+0.19	0.30	0.26	0.07	direct (M)	3.32
inside	−0.02			0.00	0.00	0.00		5.20

BLG-2CH_3	ΔE_2	Δ_{tot}	D
ud-12	−2.15	<0.01	5.16
ud-13	−0.39	<0.01	4.84
ud-14	−1.52	<0.01	5.19

[a] $\Delta E_1^{c,p}$ are chemisorption and physisorption energies, ΔE_{TS} is the transition state energy relative to the BLG+CH_3 asymptote, $\Delta_\uparrow$ ($\Delta_\downarrow$) is the spin-up (down) gap, Δ_{tot} is the total gap, and D is the distance between the two layers (in Å), as defined in Figure 5 above and Figure 12 in Appendix B. [b] ΔE_2 is defined here as the energy gain when adding a CH_3 group to BLG-1CH_3 "outside". All energies are in eV, and all calculations were done with PBE+D3.

$CH_3^- + Li^+$ (c) and SLG-2$CH_3^{2-} + 2Li^+$ (d), respectively. Apart from the counterions, the structures of SLG-1$CH_3^{\mp}$ and SLG-2$CH_3^{2-/2+}$ are similar to those of SLG-1CH_3 and SLG-2CH_3, respectively. In particular, the accepting C atoms of SLG rehybridize and pyramidalize and, for SLG-2$CH_3^{2-/2+}$, the ud-12 species are most stable, as for SLG-2CH_3. We further find some small differences in C−C bond lengths for SLG-2$CH_3^{2\pm}$ and SLG-2CH_3.

From Table 5, where first and second reaction energies are indicated, along with the total band gap and the type of calculation (e.g., spin-polarized, $M = 1$), we note the following:

(i) All reaction energies shown are large and negative, indicating exoenergetic processes. Typical reaction energies are larger than those for radicalic methylation. For CH_3Li, this is in agreement with results by Denis, who showed that lithium doping significantly increases the reactivity of monolayer graphene, enhancing the binding energy of CH_3 by about 0.66 eV.[52] The reaction energies involving CH_3Cl are more negative, by about 0.2 eV for the formation of SLG-CH_3^+ and about 1.0 eV for formation of SLG-2CH_3^{2+}, than the corresponding values for SLG-CH_3^- and SLG-2CH_3^{2-} obtained with CH_3Li. However, since the homolytic dissociation energy of CH_3Li is about 2.0 eV smaller than the dissociation energy of CH_3Cl, the overall energy balance is in favor of CH_3Li.

(ii) ΔE_2 is larger than ΔE_1 as for radicalic methylation; however, the difference between the two is not quite as striking compared to the radical route. That is, low-coverage situations (e.g., one methyl per (2 × 2) cell) should be more easily accessible via the heterolytic pathway.

(iii) For the coverages studied here (1/8 and 1/4), computed band gaps are small or zero. For two methyl groups added,

https://doi.org/10.1021/acsomega.3c02068
ACS Omega 2023, 8, 22026−22041

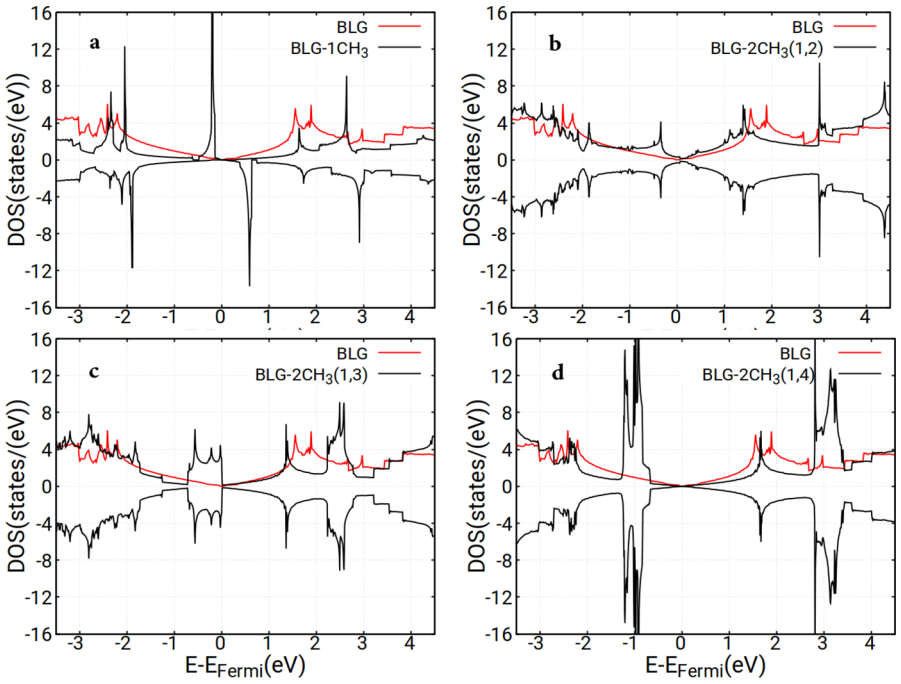

Figure 6. Electronic DOS curves for the four systems shown in Figure 5, namely, (a) BLG-1CH_3 (outside), (b) ud-12 BLG-2CH_3 (named here BLG-2CH_3(1,2)), (c) ud-13 BLG-2CH_3, and (d) ud-14 BLG-2CH_3, in comparison to the DOS of pristine BLG (red).

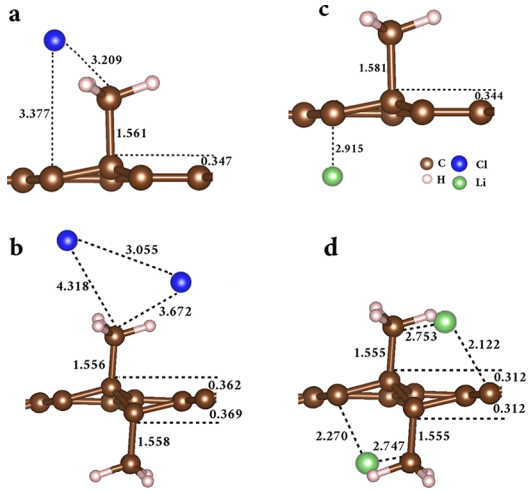

Figure 7. Optimized structures (side views) of (a) SLG-1CH_3^++Cl^-, (b) SLG-2CH_3^{2+}+2Cl^-, (c) SLG-1CH_3^-+Li^+, and (d) SLG-2CH_3^{2-}+2Li^+, all calculated on the PBE+D3 level of theory. Cl is in blue and Li in green. Some bond lengths and out-of-plane displacements are indicated.

this is in agreement with the homolytic case, whereas adding only one CH_3 *radical* led to a larger (∼0.57 eV) band gap according to Tables 2 and 3. In contrast, for SLG-1CH_3^-+Li^+ we find no gap and a very small one for SLG-1CH_3^++Cl^-.

(iv) We cannot exclude that the very small or zero gaps are caused by incomplete charge transfer. Calculating Bader atomic charges[53] at the PBE+D3 level using VASP, we find for SLG-CH_3^-+Li^+ and SLG-2CH_3^-+2 Li^+ that the charge transfer from the Li subsystem to the methylated graphene system is 0.43 and 1.72 *e*, respectively. Similarly, for SLG-CH_3^++Cl^- and SLG-2CH_3^{2+}+2 Cl^- we have charge transfer of 0.44 and 0.58 *e* from the methylated SLG to the Cl subsystem, respectively. It is presently not clear if the incomplete charge transfer, which also causes zero or very small gaps, is due to the (DFT) methods used here or a physical feature of the low-dimensional system under study. HSE06+D3 calculations on the PBE+D3-optimized SLG-1CH_3^-+Li^+ and SLG-1CH_3^++Cl^- structures also result in very small gaps, and Bader charges are very similar to the PBE+D3 values.

In addition to the systems studied in Figure 7 and Table 5, we also considered other structures arising from heterolytic functionalization, other spin multiplicities and, finally, also the heterolytic functionalization of BLG. Some findings for those systems and settings are described in Appendix C.

Table 5. Reaction of Single or Two CH_3 Cations or Anions with SLG[a]

system	1CH_3^++Cl^-	1CH_3^-+Li^+	system	2CH_3^{2+}+2Cl^- (ud-12)	2CH_3^{2-}+2Li^+ (ud-12)
ΔE_1	−1.43	−1.20	ΔE_2	−4.36	−3.37
Δ_{tot}	0.04	<0.01	Δ_{tot}	<0.01	<0.01
mode	spin-polarized[b] (M = 1)	spin-polarized[b] (M = 1)	mode	spin-polarized (M = 1)	spin-polarized[b] (M = 1)

[a]Also taking the counterions into account. Shown are first and second reaction energies, ΔE_1 and ΔE_2, respectively, the latter of which computed by adding CH_3Cl/Li to the most stable single-methylated species, SLG-1$CH_3^{\pm}$+Cl^-/Li^+. All for (2 × 2) unit cells. All energies refer to the structures shown in Figure 7, calculated using PBE+D3. Computed total gaps Δ_{tot} and computation mode are also shown. All energies are in eV. [b]Almost the same as spin-unpolarized, M = 1.

https://doi.org/10.1021/acsomega.3c02068
ACS Omega 2023, 8, 22026−22041

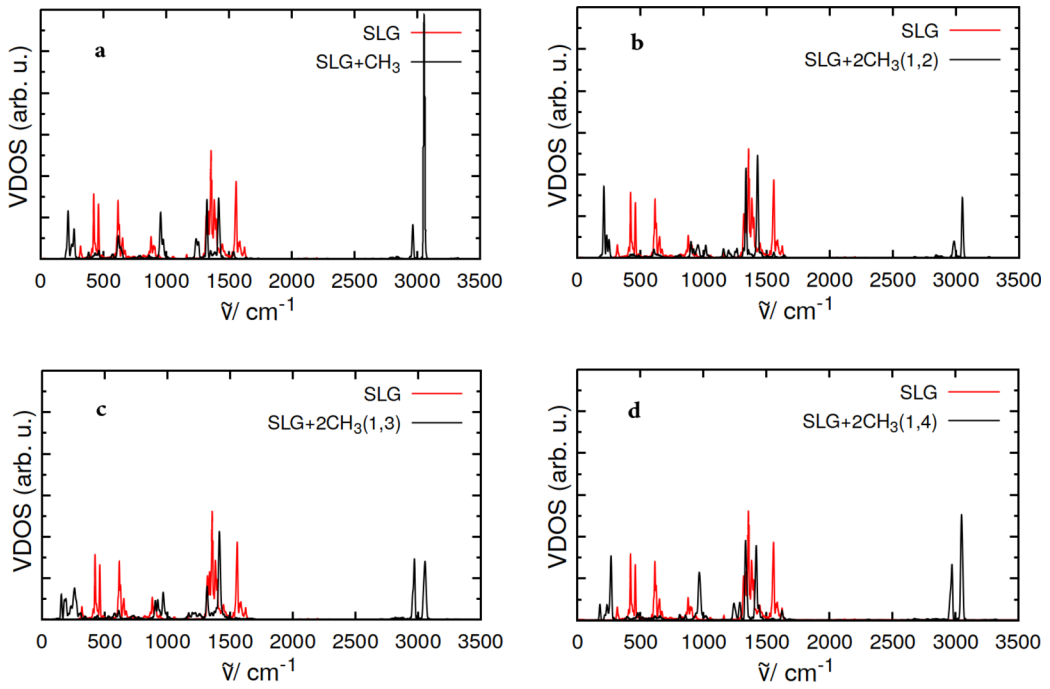

Figure 8. VDOS for pristine SLG (red curves) and methylated systems (black curves) obtained from AIMD/NVT at 298.15 K: (a) SLG-1CH_3, (b) SLG-2CH_3 (ud-12), (c) SLG+2CH_3 (ud-13), and (d) SLG+2CH_3 (ud-14).

3.6. Vibrational Spectra for Methylated SLG and BLG.

We have seen a great variety of structures and compositions of homolytically or heterolytically methylated SLG and BLG from DFT calculations. The question arises how these different forms could be disentangled experimentally. Here we briefly study one possibility to do so, namely through the vibrational signatures of these materials, probed by vibrational spectroscopy.

Let us start with SLG, methylated with one or two methyl radicals, as studied in section 3.1 and 3.2. In Figure 8, we show VDOS curves obtained from AIMD calculations at 298.15 K as described in section 2.2 using eq 1. The VDOS curves are shown for SLG-1CH_3 and SLG-2CH_3, the latter for ud-12, ud-13, and ud-14, all in comparison to the VDOS curve of SLG.

Considering pristine SLG first, we see from the figure that vibrations of the carbon lattice extend up to ∼1600 cm^{-1}, with a maximum around 1300−1400 cm^{-1} and a smaller VDOS toward lower frequencies. When adding CH_3 (see Figure 8(a)), the most striking effects are due to the appearance of new features, most notably around 2950 and 3100 cm^{-1} (C−H symmetric and asymmetric stretches, respectively), at 1350−1450 cm^{-1} (H−C−H scissor and umbrella modes), and around 1000 cm^{-1} (CH_3 rocking). Further, there is the C−CH_3 stretching modes (around 650 cm^{-1}). This assignment is based on analysis done in Appendix D in Table 6, where we also compare characteristic AIMD peaks to a normal-mode analysis. The latter does not account for anharmonicity and temperature effects, though. Apart from the new peaks, we also find that the graphene C−C vibrations shift somewhat and can have different intensities compared to pristine SLG. Adding a second CH_3 group (Figure 8(b)) has some small effects. According to Table 6, the most prominent quantitative effect (apart from intensities) when going from SLG-1CH_3 to SLG-2CH_3 (ud-12) is a ∼50 cm^{-1} blueshift of the H−C−H scissoring mode(s) between 1400 and 1500 cm^{-1}. Further, the VDOS curves of all double-functionalized species are similar. Closer inspection shows that the most obvious distinction between SLG-2CH_3 (ud-12) on the one side, and SLG-2CH_3 (ud-13) and SLG-2CH_3 (ud-14) on the other is through the CH_3 rocking mode(s) around and above 1000 cm^{-1}, which are blue-shifted for the latter two by ∼70 cm^{-1} compared to the former, cf. Table 6.

In Figure 13 in Appendix D, it is shown that similar conclusions hold for computed IR spectra, calculated by the AIMD-VVAF method as described in section 2.2. That is, for *z*-polarized IR spectra, the most striking features are intensity changes when going from single- to double-methylation, or when comparing different double-functionalized species. Further, there are similar peak shifts as for the VDOS. Note that in our approach computed IR spectra will only represent the C−C vibrations reliably. Still, C−H vibrations can also be seen due to the fact that in AIMD all modes are coupled. Finally, for completeness, we show in Appendix D, in Figures 14 and 15, VDOS curves and IR spectra for selected other systems studied in this work, with heterolytic $CH_3^{\pm}$ functionalization and or functionalization of BLG.

4. SUMMARY AND CONCLUSIONS

Here we studied the methylation of SLG and BLG via "homolytic" (reactions with CH_3 radicals) and "heterolytic" pathways (reactions with CH_3 anions or cations). Besides structures and reaction energies, properties such as band gaps and vibrational signatures were also computed, all with PBE+D3 using periodic supercell models. The most important findings are as follows.

- Low-coverage radicalic methylation of SLG is exoenergetic, with weak physisorption wells and deeper chemisorption wells separated by small barriers. The chemisorption with an odd number of CH_3 radicals (per unit cell) is energetically less favorable than situations with an even number of CH_3 radicals, for which "dangling electrons" can pair up to create stable species, such as in ud-12, for example. During chemisorption, accepting C atoms of SLG rehybridize to sp^3, and both the accepting C

https://doi.org/10.1021/acsomega.3c02068
ACS Omega 2023, 8, 22026−22041

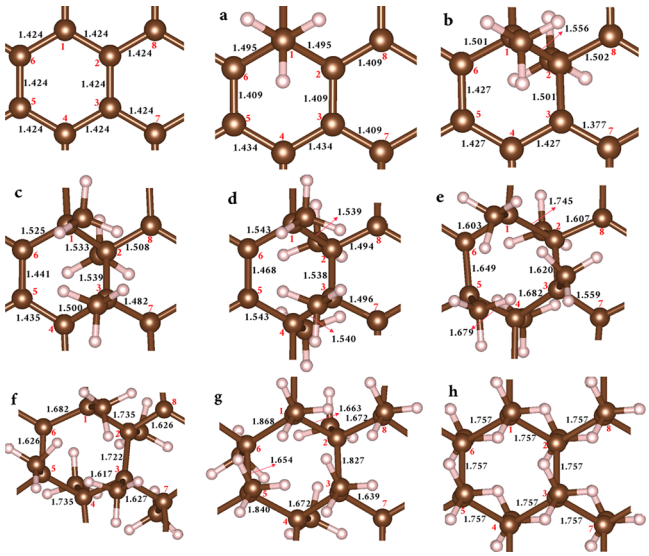

Figure 9. (a–h) Top view of optimized most-stable found structures of SLG-nCH$_3$ (from n = 0 to n = 8) for (2 × 2) unit cells used in this work. The structure of SLG in comparison is shown in the upper left corner. For n = 1–4, the lattice parameters were fixed at $a = b$ = 4.93 Å and γ = 120° (the optimized values for n = 0, i.e., free-standing SLG), while for crowded n = 5–8 the lattice parameters have been reoptimized (see text). Bond lengths (in Å) are also indicated. All calculations were done using spin-polarized PBE+D3 for multiplicities M = 2 (in the case of n = 1 (a), 3 (c), 5 (e), and 7 (g)) and M = 1 (in the case of n = 2 (b), 4 (d), 6 (f), and 8 (h)).

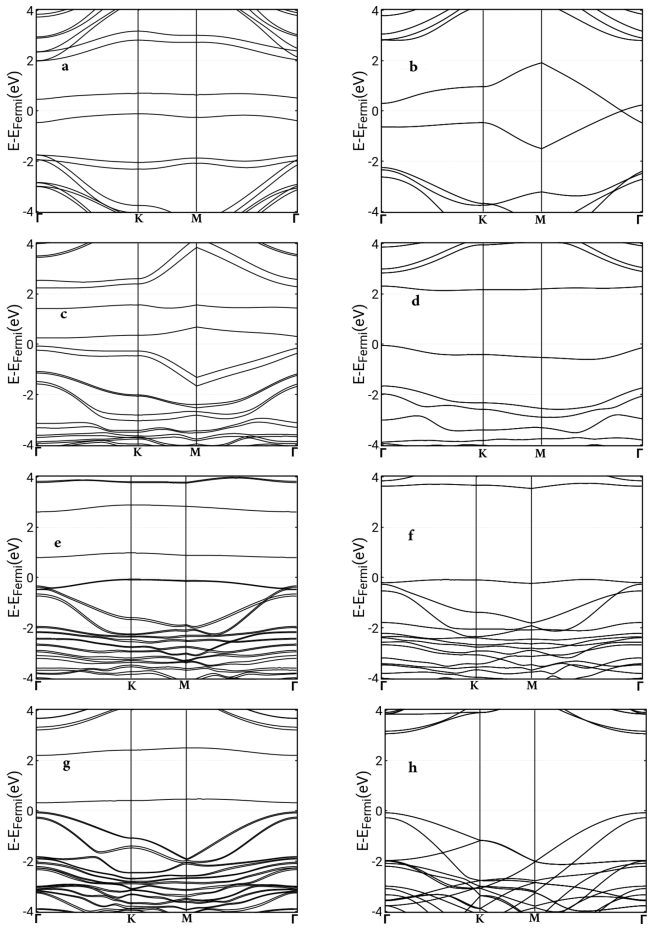

Figure 10. (a–h) Band structures of optimized most-stable found structures of SLG-nCH$_3$ (from n = 1 to n = 8) for (2 × 2) unit cells used in this work. All calculations were done using spin-polarized PBE+D3 for multiplicities M = 2 (in the case of n = 1 (a), 3 (c), 5 (e), and 7 (g)) and M = 1 (in the case of n = 2 (b), 4 (d), 6 (f), and 8 (h)).

atoms and the methyl C adopt pyramidal (nonflat) local geometries. When functionalizing with increasing amounts of methyl, alternating "up–down" structures are formed (due to reducing the deformation energy necessary for the functionalization) up to full saturation, this way creating a methylated analog of graphane. All of this is similar to what is found for hydrogenated graphene; however, at least the structures above a coverage of θ = 1/2 are high-energy, probably unstable, compounds with strongly elongated C–C bonds. The methylated analog of graphane, methyl-graphane, on the other hand is less unstable than its high-coverage neighbors such as SLG-5CH$_3$ to SLG-7CH$_3$.

- Like for hydrogenated graphene, an increasing degree of functionalization (methylation) converts SLG from a zero-gap semimetal to a semiconductor. At low coverage, θ = 1/4, the gap is still almost zero but then increases nonmonotonically up to ∼3.1 eV for methyl graphane on the PBE(+D3) level. We expect the band gap of methyl graphane to be smaller than that of graphane, which has a gap smaller than diamond. In almost all cases we studied, low-spin states were preferred, i.e., for the series SLG-nCH$_3$ M = 1 in the case of even n and M = 2 in the case of odd n. For the latter, the band structure appears to be spin-polarized, and interesting magnetic properties can be expected.
- Radicalic "outside" methylation of bilayer graphene shows quite similar behavior to SLG. "Inside" adsorption is less favored at low coverages due to the loss of van der Waals attraction between layers arising from large space requirements, which push the two graphene layers apart. However, with increasing degrees of methylation, alternating "up–down" (or "outside-inside") structures are favored compared to "outside–outside". Electronic and structural properties of methylated BLG are, broadly speaking, a simple combination of properties of pristine graphene weakly interacting with a functionalized SLG layer.
- Considering the "heterolytic" route to methylated SLG and BLG, by (formally) splitting CH$_3$Li and CH$_3$Cl into ion pairs and adding methyl anions or cations to the substrate, appears first of all to be energetically favorable in comparison to the "homolytic" route. Additionally, since unpaired electrons play no role, differences between odd and even numbers of methyl groups are less pronounced and spin-polarization does usually not occur. Other than that, the most stable structural motifs found are very similar to those found via the "radical route". Up to the θ = 1/4 coverages studied, only very small or no band gaps were observed for the heterolytic species.
- Methylation gives also rise to altered vibrational spectra. Several features have been identified that may be used as "fingerprints" of methylation, and, perhaps, also to quantify the degree of methylation.

In summary, we have shown that the methylation of single- and bilayer-graphene should be feasible, possibly also beyond very low coverages. The methylation can be understood as a first

https://doi.org/10.1021/acsomega.3c02068
ACS Omega 2023, 8, 22026–22041

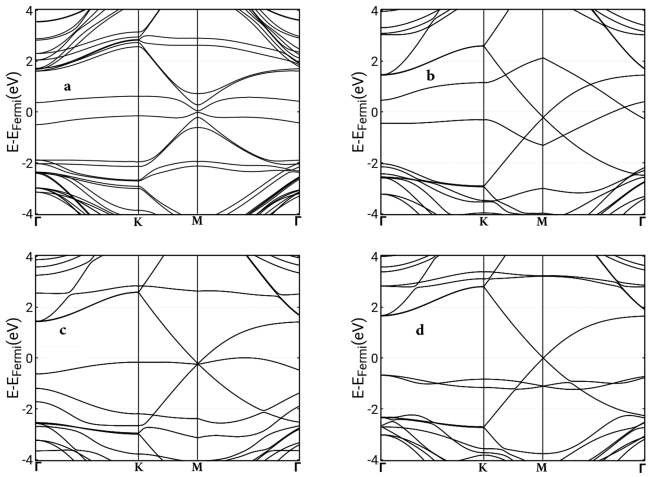

Figure 11. Band structures for the four methylated BLG systems shown in Figure 5: (a) BLG-1CH_3 (outside), (b) ud-12 BLG-2CH_3 (named here BLG-2CH_3(1,2)), (c) ud-13 BLG-2CH_3, and (d) ud-14 BLG-2CH_3. All calculations were done with PBE+D3, spin-polarized, and multiplicity equal to 2.

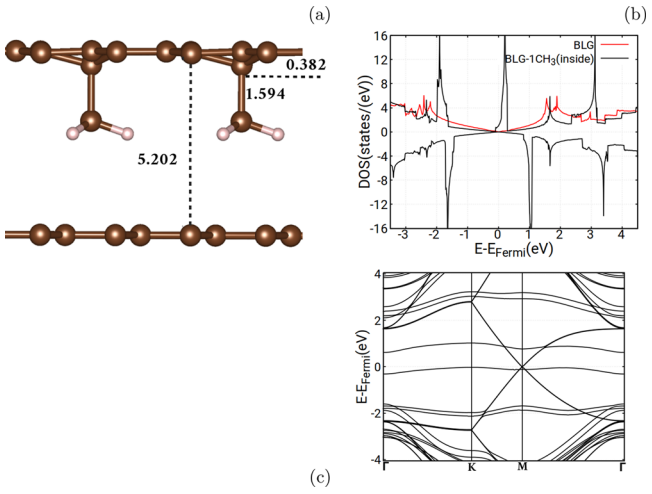

Figure 12. (a) Side view of BLG-1CH_3 (inside), optimized, with some bond lengths (in Å) indicated. (b) Corresponding electronic DOS curve for spin-up and spin-down (black) in comparison to the (spin-unpolarized) DOS of BLG (red). (c) Corresponding band structure. All calculations were done with PBE+D3, spin-polarized, and multiplicity equal to 2.

step toward the construction of C−C connected layered structures with rich structural variability and hopefully also with tunable optoelectronic properties.

APPENDICES

A. SLG Functionalized with Various Amounts of CH_3 Radicals

For graphical representations of this topic, see Figures 9 and 10.

B. BLG Functionalized with Various Amounts of CH_3 Radicals

For graphical representations of this topic, see Figures 11 and 12.

C. SLG and BLG Functionalized with CH_3 Cations or Anions: Further Findings

In section 3.5, the methylation of graphene by heterolytic reactions (methyl cations and anions) was studied. In particular, the most stable structures of SLG after functionalization with one or two methyl ions and corresponding energies and optoelectronic properties were considered (cf. Figure 7 and Table 5). In addition, we also considered other structures, other spin multiplicities and, finally, the heterolytic functionalization of BLG. Some interesting findings in this context are as follows:

(i) In all cases studied for heterolytically functionalized SLG, systems with spin multiplicity M = 1 were more stable than higher multiplicities. For example, for SLG-1CH_3^-+Li^+, a spin-polarized calculation with M = 3 gave ΔE_1 = −0.64 eV, which is about half the reaction

Table 6. Comparison and Assignment of Normal Mode Wavenumbers (in cm^{-1}) for SLG with One or Two CH_3 Radicals at the PBE+D3 Level of Theory[a]

	assignment					
structure	C−H asym str.	C−H sym str.	H−C−H sci. in CH_3	bending umbr.	CH_3-rock. on SLG	CH_3-SLG str.
SLG-CH_3	3067	2975	1545	1434	973	638
	3066		1543	1434	973	638
AIMD	3087	2945	1422	1348	1004	660
SLG-2CH_3 (ud-12)	3073	2992	1563	1442	970	618
	3072	2985		1441		
	3070			1438		
	3067			1438		
AIMD	3110	2948	1478	1363	1005	650
SLG-2CH_3 (ud-13)	3076	2978	1531	1469	998	628
	3072	2978				
AIMD	3109	2960	1468	1375	1080	640
SLG-2CH_3 (ud-14)	3065	2970	1637	1453	985	626
	3064		1636	1452	985	
	3061					
	3061					
AIMD	3105	2955	1462	1370	1078	640

[a]The entry "AIMD" gives the position of the corresponding AIMD peak (with maximal intensity).

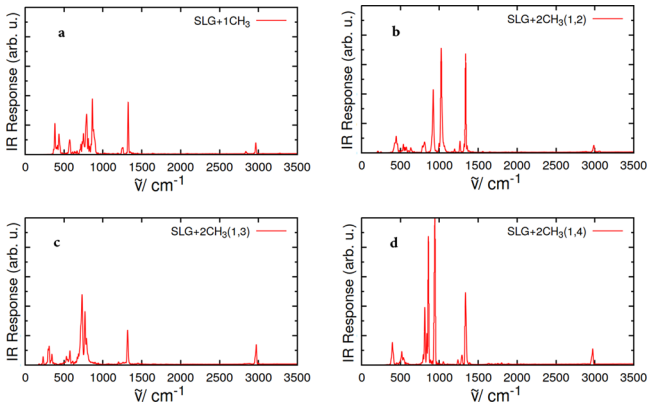

Figure 13. IR spectra (z-polarized) for methylated SLG systems obtained from AIMD/NVT at 298.15 K: (a) SLG-1CH_3, (b) SLG-2CH_3 (ud-12), (c) SLG-2CH_3 (ud-13), and (d) SLG-2CH_3 (ud-14). For the spectra, μ'_{CC} = 1 was used in eq 2. The most intense peak of the figure (the one close to 1000 cm^{-1} in panel (d)) was normalized to 1, and the same scaling was used for all other panels.

(ii) In all cases studied for heterolytically functionalized SLG, systems with spin multiplicity M = 1 were more stable than higher multiplicities. For example, for SLG-1CH_3^-+Li^+, a spin-polarized calculation with M = 3 gave ΔE_1 = −0.64 eV, which is about half the reaction

https://doi.org/10.1021/acsomega.3c02068
ACS Omega 2023, 8, 22026−22041

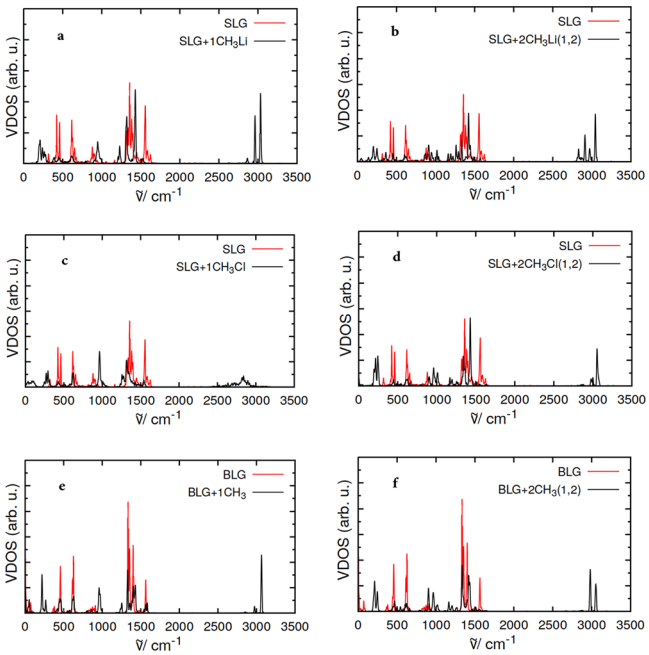

Figure 14. VDOS for pristine SLG and BLG (red curves), heterolytically methylated SLGs, and homolytically methylated BLGs (black curves) obtained from AIMD/NVT at 298.15 K: (a) SLG-1CH_3^-+Li^+, (b) SLG+2CH_3^-(1,2)+2Li^+, (c) SLG-1CH_3^++Cl^-, (d) SLG+2CH_3^+(1,2)+2Cl^-, (e) BLG-1CH_3, and (f) BLG+2CH_3(1,2). Note: the black spectrum in (b) is for a slightly less stable structure than the one shown in Figure 7(d), with both Cl atoms on one side.

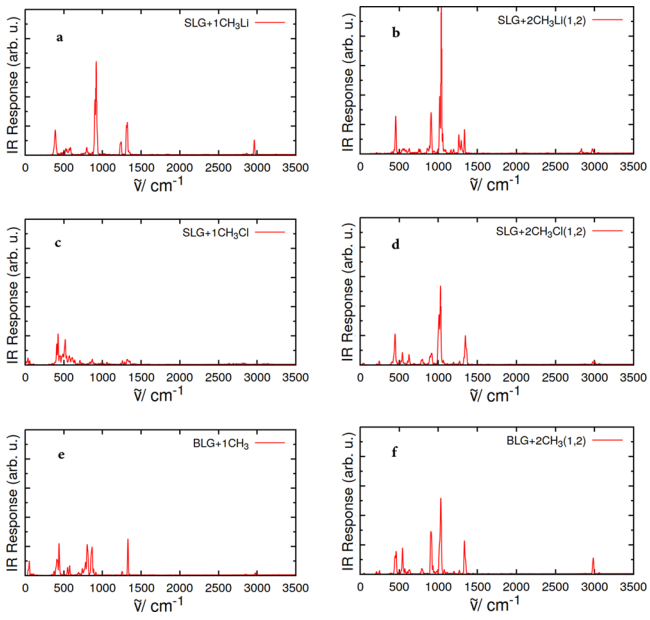

Figure 15. IR spectra corresponding to the systems considered in Figure 14: (a) SLG-1CH_3^-+Li^+, (b) SLG+2CH_3^-(1,2)+2Li^+, (c) SLG-1CH_3^++Cl^-, (d) SLG+2CH_3^+(1,2)+2 Cl^-, (e) BLG-1CH_3, and (f) BLG+2CH_3(1,2). For the spectra, μ'_{CC} = 1 was used in eq 2. The most intense peak of the figure (the one close to 1000 cm^{-1} in panel (b)) was normalized to 1, and the same scaling was used for all other panels. Note: the spectrum in (b) is for a slightly less stable structure than the one shown in Figure 7(d), with both Cl atoms on one side.

energy obtained with a spin-polarized M = 1 calculation (see Table 5).

(ii) After double-functionalization of SLG, as mentioned in the main text, the ud-12 forms are most stable compared to alternatives like ud-13, ud-14, or uu-12. For example, for SLG-2CH_3^{2-}+2Li^+, the reaction energies leading to ud-13 and ud-14 are −0.96 and −1.99 eV, respectively, compared to ΔE_1 = −3.37 eV for ud-12.

(iii) We have also studied the heterolytic methylation of BLG. For the reaction of a (2 × 2) unit cell of BLG with a single CH_3Li molecule, the most stable arrangement is CH_3^- adsorbing "outside" and Li^+ "inside" (i.e., between) the two layers, with a reaction energy ΔE_1 = −1.98 eV, which is somewhat more exoenergetic than the corresponding reaction with SLG (ΔE_1 = −1.20 eV, see Table 5). The most stable form obtained after adding a second CH_3Li is ud-12 and two Li^+ ions between the layers, with a reaction energy ΔE_2 = −2.27 eV, which is somewhat less exoenergetic than the corresponding reaction with SLG (ΔE_2 = −3.15 eV, see Table 5). The formed structures are gapless and spin-unpolarized. Similarly, for the reaction of a (2 × 2) unit cell of BLG with a single CH_3Cl molecule, the most stable arrangement is that with both CH_3^+ and Cl^- "inside". We find ΔE_1 = −1.32 eV, similar to what was found for SLG (−1.43 eV, see Table 5). Double-functionalization with CH_3Cl gives ud-12 and two Cl^- ions between the layers as the most stable structure, with ΔE_2 = −4.32 eV, again similar to the value for SLG. Here also the formed structures are gapless and spin-unpolarized.

D. Vibrational Spectra of SLG and BLG Functionalized with CH_3 Radicals, Anions, Or Cations

For data and graphical representations of this topic, see Table 6 and Figures 13−15.

AUTHOR INFORMATION

Corresponding Author

Peter Saalfrank − *Institut für Chemie, Universität Potsdam, D-14476 Potsdam, Germany; Institut für Physik und Astronomie, Universität Potsdam, D-14476 Potsdam, Germany;* orcid.org/0000-0002-5988-5945; Email: peter.saalfrank@uni-potsdam.de

Authors

Elham Mazarei − *Institut für Chemie, Universität Potsdam, D-14476 Potsdam, Germany*

Christopher Penschke − *Institut für Chemie, Universität Potsdam, D-14476 Potsdam, Germany;* orcid.org/0000-0002-0117-7479

Complete contact information is available at: https://pubs.acs.org/10.1021/acsomega.3c02068

Notes

The authors declare no competing financial interest.

ACKNOWLEDGMENTS

This work was funded by the Deutsche Forschungsgemeinschaft (DFG, German Research Foundation) under Germany's Excellence Strategy EXC 2008/1-390540038, within project Sa 548/18-1, and Projektnummer 491466077.

REFERENCES

(1) Lee, C.; Wei, X.; Kysar, J. W.; Hone, J. Measurement of the Elastic Properties and Intrinsic Strength of Monolayer Graphene. *Science* **2008**, *321*, 385−388.

(2) Xiong, R.; Hu, K.; Grant, A. M.; Ma, R.; Xu, W.; Lu, C.; Zhang, X.; Tsukruk, V. V. Ultrarobust Transparent Cellulose Nanocrystal-Graphene Membranes with High Electrical Conductivity. *Adv. Mater.* **2016**, *28*, 1501−1509.

(3) Murata, H.; Nakajima, Y.; Saitoh, N.; Yoshizawa, N.; Suemasu, T.; Toko, K. High-Electrical-Conductivity Multilayer Graphene Formed by Layer Exchange with Controlled Thickness and Interlayer. *Sci. Rep.* **2019**, *9*, 4068.

(4) Cao, M.; Xiong, D.-B.; Yang, L.; Li, S.; Xie, Y.; Guo, Q.; Li, Z.; Adams, H.; Gu, J.; Fan, T.; et al. Ultrahigh Electrical Conductivity of Graphene Embedded in Metals. *Adv. Funct. Mater.* **2019**, *29*, 1806792.

(5) Xu, X.; Pereira, L. F.; Wang, Y.; Wu, J.; Zhang, K.; Zhao, X.; Bae, S.; Bui, C. T.; Xie, R.; Thong, J. T.; et al. Length-Dependent Thermal Conductivity in Suspended Single-Layer Graphene. *Nat. Commun.* **2014**, *5*, 3689.

(6) Balandin, A. A. Thermal Properties of Graphene and Nanostructured Carbon Materials. *Nat. Mater.* **2011**, *10*, 569−581.

(7) Stoller, M. D.; Park, S.; Zhu, Y.; An, J.; Ruoff, R. S. Graphene-Based Ultracapacitors. *Nano Lett.* **2008**, *8*, 3498−3502.

(8) Reina, A.; Jia, X.; Ho, J.; Nezich, D.; Son, H.; Bulovic, V.; Dresselhaus, M. S.; Kong, J. Large Area, Few-Layer Graphene Films on Arbitrary Substrates by Chemical Vapor Deposition. *Nano Lett.* **2009**, *9*, 30−35.

(9) Nair, R. R.; Blake, P.; Grigorenko, A. N.; Novoselov, K. S.; Booth, T. J.; Stauber, T.; Peres, N. M.; Geim, A. K. Fine Structure Constant Defines Visual Transparency of Graphene. *Science* **2008**, *320*, 1308−1308.

(10) Van Noorden, R. Chemistry: The Trials of New Carbon. *Nature* **2011**, *469*, 14−16.

(11) Ramanathan, T.; Abdala, A.; Stankovich, S.; Dikin, D.; Herrera-Alonso, M.; Piner, R.; Adamson, D.; Schniepp, H.; Chen, X.; Ruoff, R.; et al. Functionalized Graphene Sheets for Polymer Nanocomposites. *Nat. Nanotechnol.* **2008**, *3*, 327−331.

(12) Si, Y.; Samulski, E. T. Synthesis of Water Soluble Graphene. *Nano Lett.* **2008**, *8*, 1679−1682.

(13) Wang, Q. H.; Hersam, M. C. Room-Temperature Molecular-Resolution Characterization of Self-Assembled Organic Monolayers on Epitaxial Graphene. *Nat. Chem.* **2009**, *1*, 206−211.

(14) He, H.; Gao, C. General Approach to Individually Dispersed, Highly Soluble, and Conductive Graphene Nanosheets Functionalized by Nitrene Chemistry. *Chem. Mater.* **2010**, *22*, 5054−5064.

(15) Pan, Y.; Bao, H.; Sahoo, N. G.; Wu, T.; Li, L. Water-Soluble Poly (N-Isopropylacrylamide)−Graphene Sheets Synthesized via Click Chemistry for Drug Delivery. *Adv. Funct. Mater.* **2011**, *21*, 2754−2763.

(16) Khan, R.; Nakagawa, R.; Campeon, B.; Nishina, Y. A Simple and Robust Functionalization of Graphene for Advanced Energy Devices. *ACS Appl. Mater. Interfaces* **2020**, *12*, 12736−12742.

(17) Vacchi, I. A.; Ménard-Moyon, C.; Bianco, A. Chemical Functionalization of Graphene Family Members. *Phys. Sci. Rev.* **2017**, *2*, 20160103.

(18) Elias, D.; Nair, R.; Mohiuddin, T.; Morozov, S.; Blake, P.; Halsall, M.; Ferrari, A.; Boukhvalov, D.; Katsnelson, M.; Geim, A.; Novoselov, K. Control of Graphene's Properties by Reversible Hydrogenation: Evidence for Graphane. *Science* **2009**, *323*, 610−613.

(19) Sofo, J. O.; Chaudhari, A. S.; Barber, G. D. Graphane: A Two-Dimensional Hydrocarbon. *Phys. Rev. B* **2007**, *75*, 153401.

(20) Sahin, H.; Leenarts, O.; Singh, S.; Peeters, F. Graphane. *WIREs Comput. Mol. Sci.* **2015**, *5*, 255−272.

(21) Gao, H.; Wang, L.; Zhao, J.; Ding, F.; Lu, J. Band Gap Tuning of Hydrogenated Graphene: H Coverage and Configuration Dependence. *J. Phys. Chem. C* **2011**, *115*, 3236−3242.

(22) Pumera, M.; Sofer, Z. Towards Stoichiometric Analogues of Graphene: Graphane, Fluorographene, Graphol, Graphene Acid and others. *Chem. Soc. Rev.* **2017**, *46*, 4450−4463.

(23) Felten, A.; Flavel, B.; Britnell, L.; Eckmann, A.; Louette, P.; Pireaux, J.-J.; Hirtz, M.; Krupke, R.; Casiraghi, C. Single- and Double-Sided Chemcial Functionalization of Bilayer Graphene. *Small* **2013**, *9*, 631−639.

(24) Biswal, M.; Zhang, X.; Schilter, D.; Lee, T.; Hwang, D.; Saxena, M.; Lee, S.; Chen, S.; Kwak, S.; Bielawski, C.; Bacsa, W.; Ruoff, R. Sodide and Organic Halides Effect Covalent Functionalization of Single-Layer and Bilayer Graphene. *J. Am. Chem. Soc.* **2017**, *139*, 4202−4210.

(25) Ke, F.; Zhang, L.; Chen, Y.; Yin, K.; Wang, C.; Tzeng, Y.-K.; Lin, Y.; Dong, H.; Liu, Z.; Tse, J. S.; Mao, W. L.; Wu, J.; Chen, B. Synthesis of Atomically Thin Hexagonal Diamond with Compression. *Nano Lett.* **2020**, *20*, 5916−5921.

(26) Liao, L.; Song, Z.; Zhou, Y.; Wang, H.; Xie, Q.; Peng, H.; Liu, Z. Photoinduced Methylation of Graphene. *Small* **2013**, *9*, 1348−1352.

(27) Li, K.; Li, N.; Yan, N.; Wang, T.; Zhang, Y.; Song, Q.; Li, H. Adsorption of Small Hydrocarbons on Pristine, N-Doped and Vacancy Graphene by DFT Study. *Appl. Surf. Sci.* **2020**, *515*, 146028.

(28) Denis, P. A.; Ullah, S.; Iribarne, F. Reduction Chemistry of Hexagonal Boron Nitride Sheets and Graphene: A Comparative Study on the Effect of Alkali Atom Doping on their Chemical Reactivity. *New J. Chem.* **2020**, *44*, 5725−5730.

(29) Kresse, G.; Joubert, D. From Ultrasoft Pseudopotentials to the Projector Augmented-Wave Method. *Phys. Rev. B* **1999**, *59*, 1758−1775.

(30) Monkhorst, H.; Pack, J. Special Points for Brillonin-Zone Integrations. *Phys. Rev. B* **1976**, *13*, 5188−5192.

(31) Perdew, J. P.; Burke, K.; Ernzerhof, M. Generalized Gradient Approximation Made Simple. *Phys. Rev. Lett.* **1996**, *77*, 3865−3868.

(32) Grimme, S.; Antony, J.; Ehrlich, S.; Krieg, H. A Consistent and Accurate Ab Initio Parametrization of Density Functional Dispersion Correction (DFT-D) for the 94 Elements H-Pu. *J. Chem. Phys.* **2010**, *132*, 154104.

(33) Grimme, S.; Ehrlich, S.; Goerigk, L. Effect of the Damping Function in Dispersion Corrected Density Functional Theory. *J. Comput. Chem.* **2011**, *32*, 1456−1465.

(34) Heyd, J.; Scuseria, G.; Ernzerhof, M. Hybrid Functionals Based on a Screened Coulomb Potential. *J. Chem. Phys.* **2003**, *118*, 8207−8215.

(35) Heyd, J.; Scuseria, G.; Ernzerhof, M. Erratum: Hybrid Functionals Based on a Screened Coulomb Potential. *J. Chem. Phys.* **2006**, *124*, 219906.

(36) Kresse, G.; Furthmüller, J. Efficiency of Ab-Initio Total Energy Calculations for Metals and Semiconductors Using a Plane-Wave Basis Set. *Comput. Mater. Sci.* **1996**, *6*, 15−50.

(37) Kresse, G.; Furthmüller, J. Efficient Iterative Schemes for Ab Initio Total-Energy Calculations Using a Plane-Wave Basis Set. *Phys. Rev. B* **1996**, *54*, 11169−11186.

(38) Nosé, S. A Molecular Dynamics Method for Simulations in the Canonical Ensemble. *Mol. Phys.* **1984**, *52*, 255−268.

(39) Berne, B.; Harp, G. On the Calculation of Time Correlation Functions. In *Advances in Chemical Physics*, Vol. *17*; Prigogine, I., Rice, S. A., Eds.; Interscience Publishers: New York, NY, 1970; p 63.

(40) Melani, G.; Nagata, Y.; Wirth, J.; Saalfrank, P. Vibrational Spectroscopy of Hydroxylated α-Al_2O_3 (0001) Surfaces with and without Water: An Ab Initio Molecular Dynamics Study. *J. Chem. Phys.* **2018**, *149*, 014707.

(41) Ohto, T.; Usui, K.; Hasegawa, T.; Bonn, M.; Nagata, Y. Toward Ab Initio Molecular Dynamics Modeling for Sum-Frequency Generation Spectra; an Efficient Algorithm Based on Surface-Specific Velocity-Velocity Correlation Function. *J. Chem. Phys.* **2015**, *143*, 124702.

(42) Henkelman, G.; Uberuaga, B. P.; Jónsson, H. A Climbing Image Nudged Elastic Band Method for Finding Saddle Points and Minimum Energy Paths. *J. Chem. Phys.* **2000**, *113*, 9901−9904.

(43) Mandeltort, L.; Choudhury, P.; Johnson, J. K.; Yates, J. T., Jr Reaction of the Basal Plane of Graphite with the Methyl Radical. *J. Phys. Chem. Lett.* **2012**, *3*, 1680−1683.

https://doi.org/10.1021/acsomega.3c02068
ACS Omega 2023, 8, 22026−22041

(44) Denis, P.; Iribarne, F. A First-Principles Study on the Interaction between Alkyl Radicals and Graphene. *Chem. Eur. J.* **2012**, *18*, 7568−7574.
(45) Tachikawa, H. Methyl Radical Addition to the Surface of Graphene Nanoflakes: A Density Functional Theory Study. *Surf. Sci.* **2019**, *679*, 196−201.
(46) Denis, P. A.; Iribarne, F. Cooperative Behavior in Functionalized Graphene: Explaining the Occurrence of 1, 3 Cycloaddition of Azomethine Ylides onto Graphene. *Chem. Phys. Lett.* **2012**, *550*, 111−117.
(47) Schreiner, P. R.; Chernish, L.; Gunchenko, P.; Tikhonchuk, E.; Hausmann, H.; Serafin, M.; Schlecht, S.; Dahl, J.; Carlson, R.; Fokin, A. Overcoming Lability of Extremely Long Alkane Carbon−Carbon Bonds through Dispersion Forces. *Nature* **2011**, *477*, 308−311.
(48) Ramakrishna, K.; Vorberger, J. Ab Initio Dielectric Response Function of Diamond and other Relevant High Pressure Phases of Carbon. *J. Phys.: Condens. Matter* **2020**, *32*, 095401.
(49) Gava, P.; Lazzeri, M.; Saitta, A. M.; Mauri, F. Ab Initio Study of Gap Opening and Screening Effects in Gated Bilayer Graphene. *Phys. Rev. B* **2009**, *79*, 165431.
(50) De Medeiros, V.; de Andrade, R.; Leitao, E.; Ventura, E.; Bauerfeldt, G.; Barbatti, M.; do Monte, S. Photochemistry of CH_3Cl: Dissociation and CH···Cl Hydrogen Bond Formation. *J. Am. Chem. Soc.* **2016**, *138*, 272−280.
(51) Schiffer, H.; Ahlrichs, R. The C-Li Bond in Methyllithium. Binding Energy and Ionic Character. *Chem. Phys. Lett.* **1986**, *124*, 172−176.
(52) Denis, P. A. Chemical Reactivity of Lithium Doped Monolayer and Bilayer Graphene. *J. Phys. Chem. C* **2011**, *115*, 13392−13398.
(53) Henkelman, G.; Arnaldsson, A.; Jónsson, H. A Fast and Robust Algorithm for Bader Decomposition of Charge Density. *Comput. Mater. Sci.* **2006**, *36*, 354−360.

https://doi.org/10.1021/acsomega.3c02068
ACS Omega 2023, 8, 22026−22041